8524 *Inorg. Chem.* **2010**, *49*, 8524–8544
DOI: 10.1021/ic101147x

Inorganic Chemistry
Article

Pnictogen-Hydride Activation by $(silox)_3Ta$ (silox = $^tBu_3SiO$); Attempts to Circumvent the Constraints of Orbital Symmetry in N_2 Activation

Elliott B. Hulley,[†] Jeffrey B. Bonanno,[†] Peter T. Wolczanski,*[,†] Thomas R. Cundari,[‡] and Emil B. Lobkovsky[†]

[†]*Department of Chemistry & Chemical Biology, Baker Laboratory, Cornell University, Ithaca, New York 14853, and* [‡]*Department of Chemistry, University of North Texas, Box 305070, Denton, Texas 76203-5070*

Received June 9, 2010

Activation of N_2 by $(silox)_3Ta$ (**1**, silox = $^tBu_3SiO$) to afford $(silox)_3Ta{=}N{-}N{=}Ta(silox)_3$ (**1**$_2$-N_2) does not occur despite $\Delta G°_{calc} = -55.6$ kcal/mol because of constraints of orbital symmetry, prompting efforts at an independent synthesis that included a study of REH_2 activation (E = N, P, As). Oxidative addition of REH_2 to **1** afforded $(silox)_3HTaEHR$ (**2**-NHR, R = H, Me, ^{n}Bu, C_6H_4-*p*-X (X = H, Me, NMe_2); **2**-PHR, R = H, Ph; **2**-AsHR, R = H, Ph), which underwent 1,2-H_2-elimination to form $(silox)_3Ta{=}NR$ (**1**=NR; R = H, Me, ^{n}Bu, C_6H_4-*p*-X (X = H (X-ray), Me, NMe_2, CF_3)), $(silox)_3Ta{=}PR$ (**1**=PR; R = H, Ph), and $(silox)_3Ta{=}AsR$ (**1**=AsR; R = H, Ph). Kinetics revealed NH bond-breaking as critical, and As > *N* > P rates for $(silox)_3HTaEHPh$ (**2**-EHPh) were attributed to (1) $\Delta G°_{calc}(N) < \Delta G°_{calc}(P) \sim \Delta G°_{calc}(As)$; (2) similar fractional reaction coordinates (RCs), but with RC shorter for $N < P{\sim}As$; and (3) stronger TaE bonds for $N > P{\sim}As$. Calculations of the pnictidenes aided interpretation of UV−vis spectra. Addition of H_2NNH_2 or $H_2N{-}N(^cNC_2H_3Me)$ to **1** afforded **1**=NH, obviating these routes to **1**$_2$-N_2, and formation of $(silox)_3MeTaNHNH2$ (**4**-$NHNH_2$) and $(silox)_3MeTaNH(\text{-}^cNCHMeCH_2)$ (**4**-NH(azir)) occurred upon exposure to $(silox)_3Ta{=}CH_2$ (**1**=CH_2). Thermolyses of **4**-$NHNH_2$ and **4**-NH(azir) yielded $[(silox)_2TaMe](\mu\text{-}N_\alpha HN_\beta)(\mu\text{-}N_\gamma HN_\delta H)$-$[Ta(silox)_2]$ (**5**) and $[(silox)_3MeTa](\mu\text{-}\eta^2\text{-}N,N{:}\eta^1\text{-}C\text{-}NHNHCH_2CH_2CH_2)[Ta(\kappa\text{-}O,C\text{-}OSi^tBu_2CMe_2CH_2)(silox)_2]$ (**7**, X-ray), respectively. $(silox)_3Ta{=}CPPh_3$ (**1**=$CPPh_3$, X-ray) was a byproduct from Ph_3PCH_2 treatment of **1** to give **1**=CH_2. Addition of Na(silox) to $[(THF)_2Cl_3Ta]_2(\mu\text{-}N_2)$ led to $[(silox)_2ClTa](\mu\text{-}N_2)$ (**8**-Cl), and via subsequent methylation, $[(silox)_2MeTa]_2(\mu\text{-}N_2)$ (**8**-Me); both dimers were thermally stable. Orbital symmetry requirements for N_2 capture by **1** and pertinent calculations are given.

Introduction

Since its discovery, $(silox)_3Ta$ (**1**, silox = $^tBu_3SiO$) has produced a remarkable array of products derived from small molecule activation because of its proclivity toward oxidative addition.[1] For example, 1/2 CO is cleaved to afford 1/2 $(silox)_3$-TaO and 1/4 $(silox)_3TaCCTa(silox)_3$,[2] and *p*-$CF_3{-}C_6H_4$-NH_2 undergoes a rare C−N bond scission to provide $(silox)_3$-$Ta(NH_2)(C_6H_4\text{-}p\text{-}CF_3)$.[3] Other activations include C−O[3,4] and E-H (E = N, P, As) bonds,[5] and the reversible addition of a CH bond at the *para*-position of 2,6-lutidine.[6] By varying the siloxide ligand, it has been shown that $^tBu_3SiO$ (silox) is unique in its ability to sterically protect the Ta(III) center of **1**,[4] thereby permitting the investigation of these activations. Interestingly, one substrate that is expected to react with **1**, dinitrogen, is noticeably absent.

Schrock's seminal studies of N_2 activation have their origins in the synthesis of $L_nX_3Ta{=}N{-}N{=}TaX_3L_n$[7−9] and related "dinitrogen" complexes, which were typically generated via the reduction of X_nM in the presence of L and N_2.[10−14] The

*To whom correspondence should be addressed. E-mail: ptw2@cornell.edu.

(1) (a) Wolczanski, P. T. *Chem. Commun.* **2009**, 740–757. (b) Wolczanski, P. T. *Polyhedron* **1995**, *14*, 3335–3362.
(2) Neithamer, D. R.; LaPointe, R. E.; Wheeler, R. A.; Richeson, D. S.; Van Duyne, G. D.; Wolczanski, P. T. *J. Am. Chem. Soc.* **1989**, *111*, 9056–9072.
(3) Bonanno, J. B.; Henry, T. P.; Neithamer, D. R.; Wolczanski, P. T.; Lobkovsky, E. B. *J. Am. Chem. Soc.* **1996**, *118*, 5132–5133.
(4) Chadeayne, A. R.; Wolczanski, P. T.; Lobkovsky, E. B. *Inorg. Chem.* **2004**, *43*, 3421–3432.
(5) Bonanno, J. B.; Wolczanski, P. T.; Lobkovsky, E. B. *J. Am. Chem. Soc.* **1994**, *116*, 11159–11160.
(6) Covert, K. J.; Neithamer, D. R.; Zonnevylle, M. C.; LaPointe, R. E.; Schaller, C. P.; Wolczanski, P. T. *Inorg. Chem.* **1991**, *30*, 2494–2508.
(7) Turner, H. W.; Fellmann, J. D.; Rocklage, S. M.; Schrock, R. R.; Churchill, M. R.; Wasserman, H. J. *J. Am. Chem. Soc.* **1980**, *102*, 7809–7811.
(8) Rocklage, S. M.; Turner, H. W.; Fellmann, J. D.; Schrock, R. R. *Organometallics* **1982**, *2*, 703–707.
(9) Rocklage, S. M.; Schrock, R. R. *J. Am. Chem. Soc.* **1982**, *104*, 3077–3081.
(10) (a) Fryzuk, M. D. *Acc. Chem. Res.* **2009**, *42*, 127–133. (b) Fryzuk, M. D.; Johnson, S. A.; Patrick, B. O.; Albinati, A.; Mason, S. A.; Koetzle, T. F. *J. Am. Chem. Soc.* **2001**, *123*, 3960–3973.
(11) (a) Gambarotta, S.; Scott, J. *Angew. Chem., Int. Ed.* **2004**, *43*, 5298–5308. (b) Gambarotta, S. *J. Organomet. Chem.* **1995**, *500*, 117–126.
(12) Chirik, P. J. *Organometallics* **2010**, *29*, 1500–1517.
(13) Lee, T.-Y.; Wooten, A. J.; Luci, J. J.; Swenson, D. C.; Messerle, L. *Chem. Commun.* **2005**, 5444–5446.
(14) Dilworth, J. R.; Henderson, R. A.; Hills, A.; Hughes, D. L.; MacDonald, C.; Stephens, A. N.; Walton, D. R. M. *J. Chem. Soc., Dalton Trans.* **1990**, 1077–1085.

 Published on Web 08/19/2010

Scheme 1

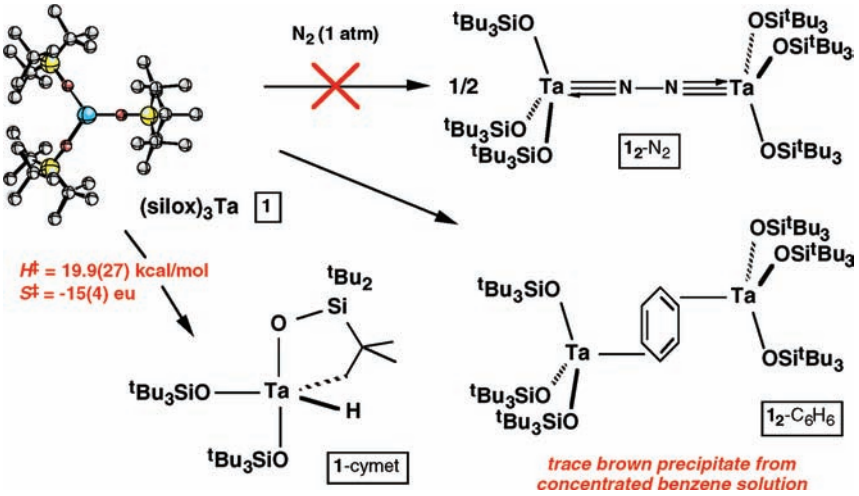

species are most aptly described as diimido complexes, as structural parameters clearly reveal the TaN multiple bonds (BO ~ 3) and N−N single bond. Given the amount of reduction of N_2 implied by the structures, it is not surprising that the compounds do not relinquish the bound "dinitrogen", even under harsh conditions. However, it is surprising that $(silox)_3Ta$ (**1**, silox = $^tBu_3SiO$), does not appear to bind dinitrogen to form $(silox)_3Ta(N_2)_x$ or reduce it to $(silox)_3Ta{=}N{-}N{=}Ta(silox)_3$ (**1**$_2$-N_2). As Scheme 1 shows, in the presence of N_2, **1** cyclometallates to afford $(silox)_2HTa(\kappa\text{-O,C-OSi-}^tBu_2CMe_2CH_2)$ (**1**-cymet),[6,15] and if sufficiently concentrated in benzene solution, a small amount is converted to the bridging benzene complex, $[(silox)_3Ta]_2(\mu\text{-}C_6H_6)$ (**1**$_2$-C_6H_6).[6,16] Since the thermodynamics, at least according to Schrock's preceding studies, certainly suggests that N_2 activation by **1** should be viable, it is likely that orbital symmetry constraints[17,18] play a crucial role in the lack of observed N_2 chemistry.[19−24] Even the cyclometalation process, which has not been shown to exhibit reversible behavior, is likely to be constrained by orbital symmetry. Herein are described attempts to circumvent these constraints and synthesize **1**$_2$-N_2 via alternate methods. In concert with these efforts, a significant study of REH_2 (E = N, P, As) oxidative addition and 1,2-H_2-elimination from $(silox)_3HTaEHR$ is also presented.[5] Computational studies support the contention that **1**$_2$-N_2 is considerably more stable than **1** and N_2.

Results

Pnictogen-Hydride Reactivity. 1. Tantalum Pnictogenide-Hydrides.[25,26] Routes to the desired dinitrogen complex can be envisaged through the oxidative addition of N−H bonds to $(silox)_3Ta$ (**1**), and Scheme 2 shows that there is ample evidence for this approach, not only for nitrogen, but for P−H and As−H bonds as well.[5,27−31] Treatment of **1** with primary amines[3,5,25,26] or ammonia[25,32] in hydrocarbon solvent (or C_6D_6 in the case of NMR tube experiments) led to the formation of $(silox)_3HTaNHR$ (**2**-NHR; R = Me, ^{n}Bu, C_6H_4-*p*-X (X = H, Me, NMe_2)) and $(silox)_3HTaNH_2$ (**2**-NH_2) in near quantitative yield (^{1}H NMR), although only the latter was isolated because of the subsequent 1,2-H_2-elimination to form the imido derivatives. An alternative synthesis involving the addition of RNH_2 to $(silox)_3TaH_2$ (**2**-H) provided **2**-NHR (R = C_6H_4-*p*-X (X = H, NMe_2, CF_3)) accompanied by the evolution of dihydrogen. IR spectra of **2**-NH_2 and **2**-NHPh revealed two and one ν(NH) stretches, respectively, and ν(TaH) stretches at 1786 cm^{-1} for the former and 1810 cm^{-1} for the latter, consistent with terminal tantalum hydrides.[33] The amide-hydrides appeared colorless, and their NMR spectra are provided in Table 1. Diagnostic, broad, amide-hydrogen resonances ranged from δ 4.56 for **2**-NH_2 to δ 7.41 for **2**-$NH(C_6H_4{-}NMe_2)$, and these were accompanied by

(15) Hirsekorn, K. F.; Veige, A. S.; Marshak, M. P.; Koldobskaya, Y.; Wolczanski, P. T.; Cundari, T. R.; Lobkovsky, E. B. *J. Am. Chem. Soc.* **2005**, *127*, 4809–4830.
(16) Neithamer, D. R.; Párkányi, L.; Mitchell, J. F.; Wolczanski, P. T. *J. Am. Chem. Soc.* **1988**, *110*, 4421–4423.
(17) Veige, A. S.; Slaughter, L. M.; Lobkovsky, E. B.; Wolczanski, P. T.; Matsunaga, N.; Decker, S. A.; Cundari, T. R. *Inorg. Chem.* **2003**, *42*, 6204–6224.
(18) Hirsekorn, K. F.; Hulley, E. B.; Wolczanski, P. T.; Cundari, T. R. *J. Am. Chem. Soc.* **2008**, *130*, 1183–1196.
(19) Cavigliasso, G.; Wilson, L.; McAlpine, S.; Attar, M.; Stranger, R.; Yates, B. F. *Dalton Trans.* **2010**, *39*, 4529–4540.
(20) (a) Laplaza, C. E.; Johnson, M. J. A.; Peters, J. C.; Odom, A. L.; Kim, E.; Cummins, C. C.; George, G. N.; Pickering, I. J. *J. Am. Chem. Soc.* **1996**, *118*, 8623–8638. (b) Figueroa, J. S.; Piro, N. A.; Clough, C. R.; Cummins, C. C. *J. Am. Chem. Soc.* **2006**, *128*, 940–950.
(21) Curley, J. J.; Cook, T. R.; Reece, S. Y.; Müller, P.; Cummins, C. C. *J. Am. Chem. Soc.* **2008**, *130*, 9394–9405.
(22) Peters, J. C.; Cherry, J.-P. F.; Thomas, J. C.; Barlado, L.; Mindiola, D. J.; Davis, W. M.; Cummins, C. C. *J. Am. Chem. Soc.* **1999**, *121*, 10053–10067.
(23) Cui, Q.; Musaev, D. G.; Svensson, M.; Sieber, S.; Morokuma, K. *J. Am. Chem. Soc.* **1995**, *117*, 12366–12367.
(24) Caselli, A.; Solari, E.; Scopelliti, R.; Floriani, C.; Re, N.; Rizzoli, C.; Chiesi-Villa, A. *J. Am. Chem. Soc.* **2000**, *122*, 3652–3670.
(25) Ammonia oxidative addition originally reported in: Neithamer, D. R., Ph.D. Thesis, Cornell University, Ithaca, NY, 1989
(26) Bonanno, J. B., Ph.D. Thesis, Cornell University, Ithaca, NY, 1996.
(27) Greenberg, S.; Stephan, D. W. *Chem. Soc. Rev.* **2008**, *37*, 1482−1489; 2798.
(28) (a) Masuda, J. D.; Hoskin, A. J.; Graham, T. W.; Beddie, C.; Fermin, M. C.; Etkin, N.; Stephan, D. W. *Chem.—Eur. J.* **2006**, *12m*, 8696–8707. (b) Stephan, D. W. *Angew. Chem., Int. Ed.* **2000**, *39*, 314–329.
(29) Shaver, M. P.; Fryzuk, M. D. *Organometallics* **2005**, *24*, 1419–1427.
(30) Tanaka, M. *Top. Curr. Chem.* **2004**, *232*, 25–54.
(31) Ebsworth, E. A. V.; Gould, R. O.; Mayo, R. A.; Walkinshaw, M. *J. Chem. Soc., Dalton Trans.* **1987**, 2831–2838.
(32) Zhao, J.; Goldman, A. S.; Hartwig, J. F. *Science* **2005**, *307*, 1080–1082.
(33) Miller, R. L.; Toreki, R.; LaPointe, R. E.; Wolczanski, P. T.; Van Duyne, G. D.; Roe, D. C. *J. Am. Chem. Soc.* **1993**, *115*, 5570–5588.

Scheme 2

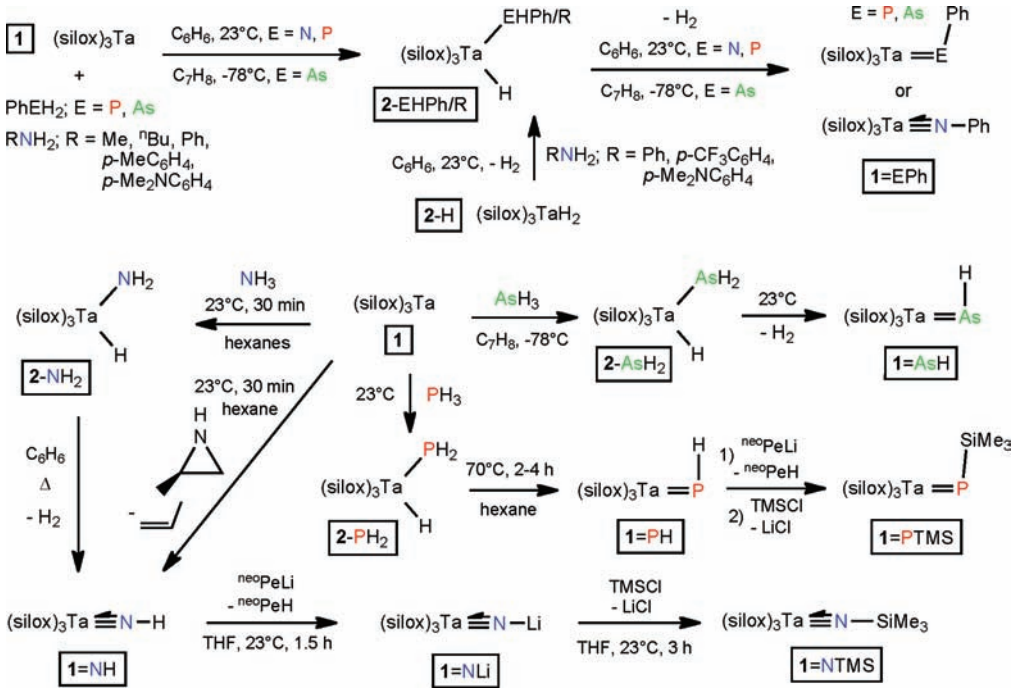

typical downfield hydride shifts ranging from δ 19.96 (**2**-NHMe) to δ 21.76 (**2**-NH(C_6H_4−CF_3)). Their structures are likely to be trigonal bipyramidal (tbp) with equatorial amide and hydride ligands or square pyramidal with basal Ta−H and Ta−NHR groups as observed for the C−N bond oxidative addition product, $(silox)_3(H_2N)TaC_6H_4$-*p*-CF_3, which was previously crystallographically characterized.[3]

The related exposure of $(silox)_3Ta$ (**1**) to $PhPH_2$ led to the formation of bright yellow $(silox)_3HTaPHPh$ (**2**-PHPh), which was crystallized from pentane in only 39% yield because of its high solubility. The parent $(silox)_3HTaPH_2$ (**2**-PH_2) complex, a pale yellow species, was isolated in 54% yield, but it was accompanied by an insoluble brick red material, which may be the double activation product $(silox)_3HTa$-PH-$TaH(silox)_3$, based on the near insolubility of the size-related, crystallographically characterized $(silox)_3Nb{=}PH$-$Nb(silox)_3$ species.[34] Phosphide **2**-PH_2 manifests ν(PH) bands at 2275 and 2285 cm^{-1} in its IR spectrum, while **2**-PHPh exhibits only one at 2320 cm^{-1}, and these were accompanied by tantalum hydride stretches at 1775 and 1790 cm^{-1}, respectively. The phenyl phosphide exhibited a ddt at δ 55.5 in its ^{31}P NMR spectrum, with $^1J_{PH}$ = 243 Hz, $^2J_{PH}$ = 56 Hz, and a coupling to the *o*-Ph hydrogens of $^3J_{PH}$ = 9 Hz. The ^{31}P NMR signal for **2**-PH_2 was very different, resonating at −142.39 ppm, with $^1J_{PH}$ = 177 Hz and $^2J_{PH}$ = 3 Hz. The difference prompted a molecular weight study of **2**-PH_2, and this was fully consistent with a monomer: M_r (found) 858(68); calcd 861. It is plausible that the two phosphide complexes possess substantially different Ta−P−R angles because of disparate steric factors, and that their chemical shifts reflect these features in addition to the electronic effects of H versus Ph. In addition, the dramatically lower $^2J_{PH}$ for **2**-PH_2 (3 vs 56 Hz) and a related, smaller $^3J_{HH}$ = 2 (vs 9 Hz for **2**-PHPh) value suggests that the geometries of the phosphide hydrides may also be different at the metal.

Preparation of the arsenide complexes proved to be trickier, as each species rapidly lost dihydrogen to form the corresponding arsinidenes. Treatment of $(silox)_3Ta$ (**1**) with $PhAsH_2$ at −78 °C in toluene-d_8 provided $(silox)_3HTaAsHPh$ (**2**-AsHPh), but the complex was stable at low temperature only if 1,4-cyclohexadiene, a radical trap, was present. Given the danger accorded the use of toxic AsH_3, it was generated via hydrolysis of Zn_3As_2 with HCl, and used immediately after passing through a cold trap. In this fashion, exposure of **1** to AsH_3 in toluene-d_8 at −78 °C, in the presence of 1,4-cyclohexadiene, afforded $(silox)_3HTaAsH_2$ (**2**-AsH_2). Characterization of the two arsenide hydrides was limited to ^1H NMR spectra at −78 °C, and the hydride resonances at δ 24.47 (d, **2**-AsHPh) and δ 24.98 (t, **2**-AsH_2) that were observed were the furthest downfield for this genre of compounds. The hydrides were coupled to AsH protons at δ 5.53 (d, $^3J_{HH}$ = 8 Hz) in **2**-AsHPh and at δ 3.13 (d, $^3J_{HH}$ = 5 Hz) in **2**-AsH_2.

2. Tantalum Pnictidene Derivatives.[35−46] The pnictidehydrides addressed in the previous section all underwent

(34) Hirsekorn, K. F.; Veige, A. S.; Wolczanski, P. T. *J. Am. Chem. Soc.* **2006**, *128*, 2192–2193.

(35) Cowley, A. H. *Acc. Chem. Res.* **1997**, *30*, 445–451.
(36) Johnson, B. P.; Balazs, G.; Sheer, M. *Top. Curr. Chem.* **2004**, *232*, 1–23.
(37) Cummins, C. C. *Angew. Chem., Int. Ed.* **2006**, *45*, 862–870.
(38) Piro, N. A.; Cummins, C. C. *J. Am. Chem. Soc.* **2009**, *131*, 8764–8765.
(39) Cossairt, B. M.; Cummins, C. C. *Inorg. Chem.* **2008**, *47*, 9363–9371.
(40) Zhao, G. Y.; Basuli, F.; Kilgore, U. J.; Fan, H. J.; Aneetha, H.; Huffman, J. C.; Wu, G.; Mindiola, D. J. *J. Am. Chem. Soc.* **2006**, *128*, 13575–13585.
(41) (a) Waterman, R.; Hillhouse, G. L. *Organometallics* **2003**, *22*, 5182–5184. (b) Melenkivitz, R.; Mindiola, D. J.; HIllhouse, G. L. *J. Am. Chem. Soc.* **2002**, *124*, 3846–3847.
(42) Sánchez-Nieves, J.; Sterenberg, B. T.; Udachin, K. A.; Carty, A. J. *J. Am. Chem. Soc.* **2003**, *125*, 2404–2405.

Table 1. NMR Spectral Assignments[a] for (silox)$_3$M Pnictogen Derivatives and Selected IR Data

	^{1}H NMR (δ (J(Hz))		^{13}C{^{1}H} NMR (δ (J(Hz))		
compound	^{t}Bu	H/ER	CMe_3,$C(CH_3)_3$	ER/R	^{31}P/^{15}N NMR (δ (J(Hz)) and IR (cm^{-1})
(silox)$_3$HTaNH$_2$ (**2**-NH$_2$)	1.29	4.56 20.04	23.83, 30.83		−229.37 (td, 72[b],5[c]) 1786, ν(TaH) 3363, ν(NH) 3453, ν(NH)
(silox)$_3$HTaNHMe (**2**-NHMe)	1.31	3.34 (d,7) 5.42 (q,7) 19.96			
(silox)$_3$HTaNH^{n}Bu (**2**-NH^{n}Bu)[d]	1.32	0.85 (t, CH_3) 3.85 (dd, NCH_2) 5.66 (t, NH) 19.99			
(silox)$_3$HTaNHPh (**2**-NHPh)[e]	1.26	6.76 (m, *p*-H) 7.15−7.26 (m, *o*-,*m*-H) 7.29 (NH) 21.47			1810, ν(TaH) 3350, ν(NH)
(silox)$_3$HTaNH(C$_6$H$_4$-*p*-Me)[e] (**2**-NHC$_6$H$_4$-*p*-Me)	1.28	2.17 (*p*-Me) 6.99 (m, *o*-,*m*-H) 7.33 (NH) 21.38			
(silox)$_3$HTaNH(C$_6$H$_4$-*p*-NMe$_2$)[e] (**2**-NHC$_6$H$_4$-*p*-NMe$_2$)	1.30	2.55 (NMe$_2$) 6.66 (d, *m*-H) 7.03 (d, *o*-H) 7.41 (NH) 21.13			
(silox)$_3$HTaNH(C$_6$H$_4$-*p*-CF$_3$)[e] (**2**-NHC$_6$H$_4$-*p*-CF$_3$)	1.23	6.91 (d, *m*-H) 7.04 (NH) 7.43 (d, *o*-H) 21.76			
(silox)$_3$Ta(NH$_2$)$_2$ (**3**-(NH$_2$)$_2$)	1.30	4.14			−241.62 (t, 71[b])
(silox)$_3$HTaPH$_2$ (**2**-PH$_2$)	1.28	2.40 (dd,177,[f] 2) 21.72 (dt,3[g], 2)	23.75, 30.65		−142.39 (td,177[f], 3[g]) 1775, ν(TaH) 2275, ν(PH) 2285, ν(PH)
(silox)$_3$HTaPHPh (**2**-PHPh)[e,i]	1.26	6.88 (t, *p*-H) 7.21 (dd,243,[f] 9) 7.72 (t,*o*-H, 9) 21.62 (dd,56,[g] 9)	23.58, 30.66	126.31 127.53 127.61 132.51 (8)[j]	55.5 (ddt,243[f], 56[g],9[h]) 1790, ν(TaH) 2320, ν(PH)
(silox)$_3$HTaAsH$_2$ (**2**-AsH$_2$)	1.29	3.13 (d,5) 24.98 (t,5)			
(silox)$_3$HTaAsHPh (**2**-AsHPh)[c]	1.26	5.53 (d, 8) 6.96 (m, *p*-H) 7.84 (d, *o*-H) 24.47 (d,8)			
(silox)$_3$Ta=NH (**1**=NH)	1.29	6.01 (br)[k]	23.78, 30.65		−60.60 ($^1J_{NH}$ = 76) 3470, ν(NH)
(silox)$_3$(H$_3$N)Ta=NH (**1**=NH(NH$_3$))	1.28	0.80 (br, NH_3) 5.67 (br, NH)			
(silox)$_3$Ta=NLi (**1**=NLi)[l]	1.20		24.40, 31.43		
(silox)$_3$Ta=NCH$_3$ (**1**=NMe)	1.29	3.89	23.42, 30.54	47.88	
(silox)$_3$Ta=N^{n}Bu (**1**=N^{n}Bu)[m]	1.29	0.92 (t, CH_3) 1.60 (m, CH_2) 4.23 (t, NCH_2)			
(silox)$_3$Ta=NSiMe$_3$ (**1**=NTMS)	1.28	0.28	23.59, 30.66	3.79	
(silox)$_3$Ta=NPh (**1**=NPh)[e]	1.27	6.75 (m, *p*-H) 7.16−7.25 (*o*-,*p*-H)	23.36, 30.55	121.82 125.35 128.31 129.41	
(silox)$_3$Ta=N(C$_6$H$_4$-*p*-Me)[e] (**1**=N(C$_6$H$_4$-*p*-Me))	1.28	2.14 (Me) 6.99 (d, *m*-H) 7.08 (d, *o*-H)			
(silox)$_3$Ta=N(C$_6$H$_4$-*p*-NMe$_2$)[e] (**1**=N(C$_6$H$_4$-*p*-NMe$_2$))	1.31	2.50 (NMe$_2$) 6.62 (d, *m*-H) 7.13 (d, *o*-H)	23.41, 30.62	40.92 113.04 125.85 146.31 150.07	
(silox)$_3$Ta=N(C$_6$H$_4$-*p*-CF$_3$)[e]	1.24	7.01 (d, *m*-H)	23.35, 30.50	123.05 ($^2J_{CF}$ = 32)	

Table 1. Continued

compound	^{1}H NMR (δ (J(Hz))		^{13}C{^{1}H} NMR (δ (J(Hz))		^{31}P/^{15}N NMR (δ (J(Hz)) and IR (cm^{-1})
	^{t}Bu	H/ER	CMe_3,$C(CH_3)_3$	ER/R	
(**1**=N(C_6H_4-*p*-CF_3))		7.38 (d, *o*-H)		125.21 125.45 ($^1J_{CF}$ = 271) 125.78 ($^3J_{CF}$ = 4) 160.33	
(silox)$_3$Ta=CH_2 (**1**=CH_2)	1.28	6.66	23.75, 30.59	185.02 (135)	
(silox)$_3$Ta=C=PPh_3 (**1**=CPPh_3)	1.31	7.71 (m, *m*,*p*-H) 7.78 (m, *o*-H)	25.21, 31.31	128.75 (*p*) 131.15 (*m*) 133.94 (*o*) 136.37 (d, 88) 175.01 (d, 53)	−4.26
(silox)$_3$Ta=PH (**1**=PH)	1.30	3.57 (d,82[f])			276.33 (d,82[f]) 2150, ν(PH)
(silox)$_3$Ta=PPh (**1**=PPh)[e]	1.28	6.76 (*m*-H[h]) 7.20 (*o*-H) 7.67 (*p*-H)	23.75, 30.61	125.79 127.67 128.29 137.27 (10[i])	334.6 (t,6[h])
(silox)$_3$Ta=$PSiMe_3$ (**1**=PTMS)	1.34	0.47 (d,6[k])			196.07
(silox)$_3$Ta=AsH (**1**=AsH)	1.30	2.04			1950, ν(AsH)
(silox)$_3$Ta=AsPh (**1**=AsPh)[e]	1.29	6.81 (*m*-H) 7.21 (*o*-H) 7.86 (*p*-H)		125.83 127.93 139.61 142.59	
(silox)$_3$Ta(AsH_2)$_2$ (**3**-(AsH_2)$_2$)	1.23	2.33			2180, ν(AsH) 2190, ν(AsH)
(silox)$_3$MeTaNHNH_2 (**4**-NHNH_2)	1.26	1.03 (Me) 3.63 (NH_2) 4.11 (NH)	23.78, 30.43	33.79	64.80 (NH_2, 78)[n] 148.47 (NH, 78)[n]
(silox)$_3$MeTaNH([c]NCH_2CMeH) (**4**-NH(azir))		1.06 (d,6,CH_3) 1.24 (d,8,CHMe) 1.44 (dd,8,4,CH*H*) 1.54 (d,4,C*H*H)			81.99 ([c]N)[n] 244.46 (NH, 72)[n,o]
[(silox)$_2$TaMe][(silox)$_2$Ta] (μ-$N_\alpha HN_\beta$)(μ-$N_\gamma HN_\delta$H) (**5**)	1.24 1.26 1.28 1.30	1.21 (Me) 3.00 (N_γH) 5.42 (N_αH) 6.38 (N_δH)	24.01, 30.83 24.10, 30.88 24.15, 31.04 24.49, 31.11	38.31	79.50 (N_γH, 72)[n,o] 131.27 (N_αH, 72)[n,o] 179.70 (N_δH, 75)[n,o] 298.23 (N_β, 8)[n,p]
[(silox)$_2$ClTa]$_2$(μ-N_2) (**8**-Cl)	1.26		23.76, 30.39		
[(silox)$_2$MeTa]$_2$(μ-N_2) (**8**-Me)	1.24	1.24	23.79, 30.44	33.87	

[a] Benzene-d_6 unless otherwise noted. [b] $^1J_{15NH}$. [c] $^3J_{15NH}$. [d] β-CH_2 and γ-CH_2 obscured. [e] All couplings between *o*-, *m*-, and *p*-Ph positions are 8(1) Hz. [f] $^1J_{PH}$. [g] $^2J_{PH}$. [h] $^3J_{PH}$. [i] *m*-H obscured. [j] $^1J_{PC}$. [k] At 80 °C, a 1:1:1 triplet due to $^1J_{14NH} \sim 50$ Hz was observed. [l] THF-d_8. [m] CH_2 obscured. [n] Obtained via HMBCAD correlation spectroscopy. [o] $^1J_{15NH}$. [p] $^2J_{15NH}$.

1,2-H_2-elimination to form the corresponding imido (nitrene) derivatives (silox)$_3$Ta=NR (**1**=NR; R = H, Me, ^{n}Bu, C_6H_4-*p*-X (X = H, Me, NMe_2, CF_3)), phosphinidenes (silox)$_3$Ta=PR (**1**=PR; R = H, Ph) and arsinidenes (silox)$_3$Ta=AsR (**1**=AsR; R = H, Ph). An alternate preparation of **1**=NH from 2-methylaziridene proved to be convenient. While the imido derivatives were colorless, (silox)$_3$Ta=PH (**1**=PH) was isolated as pale orange crystals (61%), and red-violet crystals of (silox)$_3$Ta=PPh (**1**=PPh)[5] were obtained in 62% yield. Parent arsinidene (silox)$_3$Ta=AsH (**1**=AsH) was isolated as dark orange crystals, but proved to be contaminated by a compound tentatively identified as (silox)$_3$Ta(AsH_2)$_2$ (**3**-(AsH_2)$_2$; ν(AsH) = 2180, 2190 cm^{-1}), which comprised ~10% of the material. A red insoluble material also formed, and this is likely to be a dinuclear substance, as speculated for the related phosphorus chemistry above.[34] It is likely that **3**-(AsH_2)$_2$ forms from reaction of excess AsH_3 in solution with (silox)$_3$HTaAsH_2 (**2**-AsH_2) via the loss of H_2, or via the 1,2-AsH-addition to the Ta=As bond of **1**=AsH. Phenylarsinidene[46] (silox)$_3$Ta=AsPh (**1**=AsPh)[5] was obtained as green crystals in 85% yield from hexane.

^{1}H and ^{13}C{^{1}H} NMR spectra of the pnictidenes listed in Table 1 reveal standard silox resonances and others corresponding to the R groups. The parent imide (**1**=NH), phosphinidene (**1**=PH), and arsinidine (**1**=AsH) possess varied pnictogen-hydrogen ^{1}H NMR spectral shifts. The imide proton is at δ 6.01, and upon warming to 80 °C, manifests a 1:1:1 triplet due to ^{14}N-coupling ($^1J_{N14H} \sim 50$ Hz). The PH resonance in **1**=PH is at δ 3.57

(43) Termaten, A. T.; Nijbacker, T.; Schakel, M.; Lutz, M.; Spek, A. L.; Lammertsma, K. *Organometallics* **2002**, *21*, 3196–3202.
(44) Freundlich, J. S.; Schrock, R. R.; Davis, W. M. *J. Am. Chem. Soc.* **1996**, *118*, 3643–3655.
(45) Breen, T. L.; Stephan, D. W. *J. Am. Chem. Soc.* **1995**, *117*, 11915–11921.
(46) Mosch-Zanetti, N. C.; Schrock, R. R.; Davis, W. M.; Wanninger, K.; Seidel, S. W.; O'Donoghue, M. B. *J. Am. Chem. Soc.* **1997**, *119*, 11037–11048.

with $^1J_{PH}$ = 82 Hz, and the arsinidene proton is observed at δ 2.04. The observation of large ^{14}N-coupling is indicative of the cylindrical symmetry expected for the triply bonded imido group. In contrast, the $^1J_{PH}$ for **1**=PH is substantially less than that found for the phosphide-hydride complexes, and is taken as an indication of further diminished s-character in the phosphinidene-hydrogen bond. Structural studies of $(silox)_3TaX$ species have historically been difficult to obtain or interpret because of disorder and twinning issues common to the 3-fold core, but it is likely that the Ta=EH angle (E = P, As) in **1**=EH is very close to 90°.

The addition of excess NH_3 to benzene solutions of **1**=NH caused the formation of a white solid, and ^{1}H NMR spectral analysis of the reaction mixture implicated the formation of $(silox)_3Ta(NH_2)_2$ (**3**-$(NH_2)_2$). $^{15}NH_3$ was used to obtain ^{15}N NMR data for **3**-$(^{15}NH_2)_2$, whose nitrogens were observed as a triplet ($^1J_{15NH}$ = 71 Hz) at δ −241.62. This assignment was based on the ^{15}N NMR spectrum of **2**-$^{15}NH_2$, obtained from $^{15}NH_3$ and $(silox)_3$-Ta (**1**), which resonated as a triplet of doublets as δ −229.37 ($^1J_{15NH}$ = 72 Hz; $^3J_{15NH}$ = 5 Hz). Attempts to generate equilibrium information pertaining to **1**=NH + $NH_3 \rightleftarrows$ **3**-$(NH_2)_2$ were fraught with complications that were attributed to complex equilibria,[47,48] since different van't Hoff plots were obtained at different concentrations of NH_3 in benzene.[26] It was suspected that aggregation of NH_3 in solution (1, 3, and 10 equiv) was at the origin of the unusual behavior, and no further attempts were made. Another complication concerned the formation of $(silox)_3$-(H_3N)Ta=NH (**1**=NH(NH_3)), whose imide resonance was shifted to a broad signal at δ 5.67 in its ^{1}H NMR spectrum accompanied by a broad NH_3 resonance at δ 0.80. It is suspected that the original white solid is a combination of **3**-$(NH_2)_2$ and **1**=NH(NH_3), but attempts to isolate either invariably led to ammonia loss. The ^{15}N NMR resonance at δ −60.60 (d, $^1J_{15NH}$ = 76 Hz) observed in solution is attributed to **1**=^{15}NH, but it is conceivable it is slightly shifted because of equilibria with the ammonia adduct. A switch to THF-d_8 revealed four distinct species, but the spectral signature for the fourth species, presumably **1**=NH(NH_3), continued to be questioned for lack of a signal that could be attributed with confidence to the NH_3 group.

Alternative syntheses of Me_3Si-capped imido and phosphinidene derivatives are also given in Scheme 2. Deprotonation of $(silox)_3Ta$=NH (**1**=NH) with neopentyllithium afforded the lithio-imide, $(silox)_3Ta$=NLi (**1**=NLi), in 78% yield as colorless crystals from tetrahydrofuran (THF). Subsequent silylation with TMSCl afforded the imide, $(silox)_3Ta$=$NSiMe_3$ (**1**=NTMS, 50%), again as colorless crystals. The corresponding route was also employed in the preparation of $(silox)_3Ta$=PTMS (**1**=PTMS), except that the phosphide anion[34,49] was generated in situ and silylated to produce a small amount of the phosphinidene for the sake of ^{31}P NMR spectroscopic studies. Phosphinidene ^{31}P chemical shifts for **1**=PH, **1**=PPh, and **1**=PTMS were recorded at δ 276.33, 334.6, and 196.07, respectively. While most of the pnictidene complexes were isolated and subjected to elemental analysis (**1**=ER, E = N, R = H, Me, $SiMe_3$, C_6H_4-*p*-X (X = H, CF_3); E = P, R = H, Ph; ER = AsPh), the remaining complexes were generated in situ for subsequent studies.

Table 2. UV−vis Absorptions for $(silox)_3Ta$=EPh (**1**=EPh; E = N, P, As)

1=NPh		**1**=PPh		**1**=AsPh	
λ (nm)	ε (M^{-1} cm^{-1})	λ (nm)	ε (M^{-1} cm^{-1})	λ (nm)	ε (M^{-1} cm^{-1})
215 (sh)	17,000	230 (sh)	18,800	226	21,300
246	13,300	244 (sh)	15,600	249	18,900
280 (sh)	9,700	275	15,900	270	14,800
285	9,750	300 (sh)	5,160	312	2,100
294 (sh)	9,300	361	3,880	385	3,950
		434 (sh)	650	450 (sh)	910
		553	310	602	250

3. UV−vis Spectra of Pnictidenes and Calculations. UV−vis spectra of $(silox)_3Ta$=EPh (**1**=EPh, E = N, P, As) were taken for comparison and their UV−vis absorptions are listed in Table 2. The higher energy absorption in each case is taken as an IL (intraligand) band because of comparisons with $NaOSi^tBu_3$,[6] and the mélange of bands in the 240−300 nm region are likely to be ligand-to-metal charge transfer (LMCT) bands of siloxide and pnictide character. In the cases of **1**=PPh and **1**=AsPh, low energy bands of relatively lower intensity are seen, whereas no features are observed below ∼330 nm for **1**=NPh. Calculations reveal the highest occupied molecular orbitals (HOMOs) of **1**=PPh and **1**=AsPh to be essentially the Ta=E π-bonding orbitals (Figure 1). The weak 553 nm (ε = 310 M^{-1} cm^{-1}) absorption of **1**=PPh is roughly 9−10,000 cm^{-1} lower[50] than the 361 nm absorption of considerably greater intensity (ε = 3,880 M^{-1} cm^{-1}), suggesting that these are the triplet and singlet bands corresponding to TaP(π^b)→Ta(d_{xz}(π^{nb})) LMCT. The modest intensities speak to the minimal overlap of the roughly orthogonal $d\pi_{yz}{}^b$ and d_{xz} orbitals. The shoulder at 300 nm and the low intensity band at 434 nm could be the TaP-(π^b)→Ta(d_{yz}(π^*)) LMCT and its accompanying triplet absorption, but computationally a $P(3s/3p_z)^{nb}$→Ta(d_{xz}-(π^{nb})) LMCT would also be a reasonable fit from both energy and intensity standpoints. Strong parallels are observed in the low energy features of **1**=AsPh, such as a weak 602 nm band (ε = 250 M^{-1} cm^{-1}) that is ∼9−10,000 cm^{-1} below a 385 nm band of modest intensity (ε = 3,950 M^{-1} cm^{-1}), which are consistent with triplet and singlet absorptions pertaining to the related to TaAs-(π^b)→Ta(d_{xz}(π^{nb})) LMCT. The assignment of the remaining low energy transitions as TaP(π^b)→Ta(d_{yz}-(π^{nb})) or $As(4s/4p_z)^{nb}$→Ta(d_{xz}(π^{nb})) singlet or triplet LMCT bands also parallels the phosphinidene case. Related interpretations of similar chalcogenide features have been made.[51,52]

The surprising feature to the calculations of $(silox)_3$-Ta=EPh (**1**=EPh, E = N, P, As) shown in Figure 1 are

(47) Roberts, J. H.; Bettignies, B. J. D. *J. Phys. Chem.* **1974**, *78*, 2106–2109.
(48) Wanna, J.; Menapace, J. A.; Bernstein, E. R. *J. Chem. Phys.* **1986**, *85*, 1795–1806.
(49) (a) Figueroa, J. S.; Cummins, C. C. *Angew. Chem., Int. Ed.* **2004**, *43*, 984–988. (b) Figueroa, J. S.; Cummins, C. C. *J. Am. Chem. Soc.* **2004**, *126*, 13916–13917.
(50) Kuiper, D. S.; Douthwaite, R. E.; Mayol, A.-R.; Wolczanski, P. T.; Lobkovsky, E. B.; Cundari, T. R.; Lam, O. P.; Meyer, K. *Inorg. Chem.* **2008**, *47*, 7139–7153.
(51) Paradis, J. A.; Wertz, D. W.; Thorp, H. H. *J. Am. Chem. Soc.* **1993**, *115*, 5308–5309.
(52) Murphy, V. J.; Parkin, G. *J. Am. Chem. Soc.* **1995**, *117*, 3522–3528.

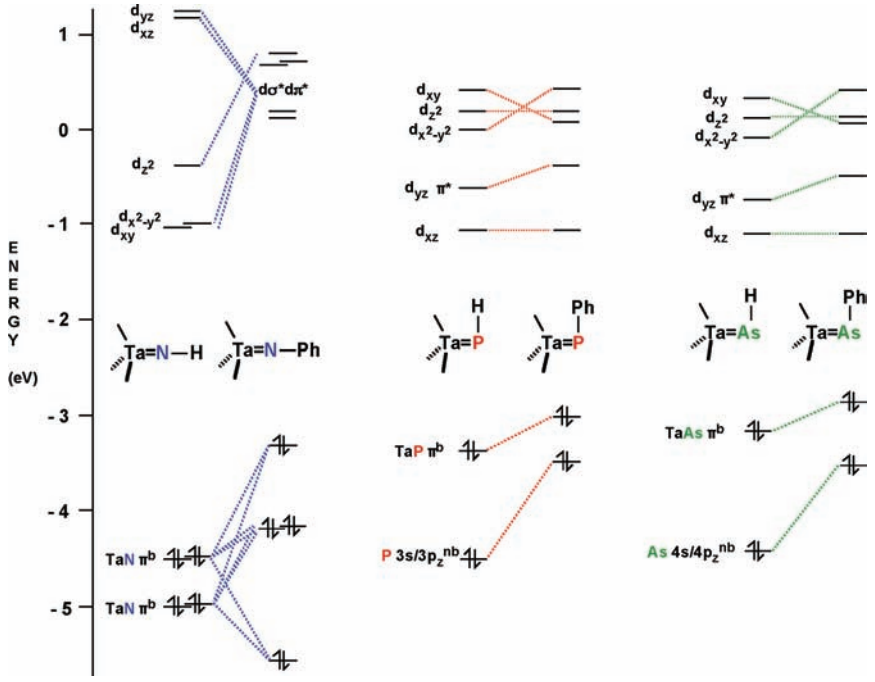

Figure 1. Truncated molecular orbital diagrams featuring pertinent Ta=E occupied levels and the ligand fields for $(silox)_3Ta{=}ER$ (**1**=ER; E = N, P, As; R = H, Ph). In all cases, the orbital parentage has been tentatively interpreted from orbital pictures, but the low symmetry (C_s) cases were difficult, and the d_{xz}/d_{yz} set mixed with the $d_{x^2-y^2}/d_{xy}$ set in **1**=NPh to such an extent that no assignment could be made. Note that the two π-bonds in **1**=NH are spread among four orbitals because of σ/π-mixing, and are further split in **1**=NPh because of mixing with the phenyl orbitals.

the HOMOs of the phosphinidene and arsenidine, which are the Ta=E π-bonding orbitals. The "lone pairs" or "inert pairs" on P and As are expected to be relatively low in energy, and the π-bonds in the system are so weak that the Ta=E bonding orbitals are not driven below the inert pairs. Clearly the large 3s/3p and 4s/4p energy gaps for elemental phosphorus and arsenic, the origin of the so-called inert pair effect,[53−56] are revealed relative to the π-interaction energies.

4. Pnictidene Structural Studies and Calculations. Crystallographic studies of $(silox)_3Ta{=}PPh$ (**1**=PPh, d(TaP) = 2.317(4) Å, ∠Ta=P−C = 110.2(4)°) and $(silox)_3$-Ta=AsPh (**1**=AsPh, d(TaAs) = 2.428(2) Å, ∠Ta=As−C = 107.2(4)°) have been reported.[5] A molecular view of $(silox)_3Ta{=}NPh$ (**1**=NPh,) and selected geometric parameters are given in Figure 2, and crystallographic details are given in Table 3. In contrast to the Ta−E−C angles of the phophinidene and arsinidene, the TaNPh linkage is essentially linear, and the tantalum−nitrogen distance is standard for a triple bond (d(TaN) = 1.767(10) Å, ∠Ta=N−C = 172.4(8)°).[57] Utilization of the 2s orbital of N in the imide linkage is therefore apparent, constituting persuasive evidence for sp hybridization. High level quantum mechanical calculations of $(silox)_3Ta{=}EPh$ (**1′**=EPh, primes indicated calculated values) are consistent with the reported structures: **1′**=NPh, d(TaN) = 1.81 Å, ∠Ta=N−C = 176.0°; **1′**=PPh, d(TaP) = 2.36 Å, ∠Ta=P−C = 112.7°; **1′**=AsPh, d(TaAs) = 2.47 Å, ∠Ta=As−C = 109.4°. Related calculations of $(silox)_3Ta{=}EH$ (**1′**=EH) show the Ta=E−H angles to be close to 90° for E = P and As, therefore steric factors probably cause the Ta=E−C angles for **1**/**1′**=PPh and **1**/**1′**=AsPh to deviate from 90°: **1′**=NH, d(TaN) = 1.79 Å, ∠Ta=N−H = 179.4°; **1′**=PH, d(TaP) = 2.36 Å, ∠Ta=P−H = 87.6°; **1′**=AsH, d(TaAs) = 2.46 Å, ∠Ta=As−H = 87.0°.

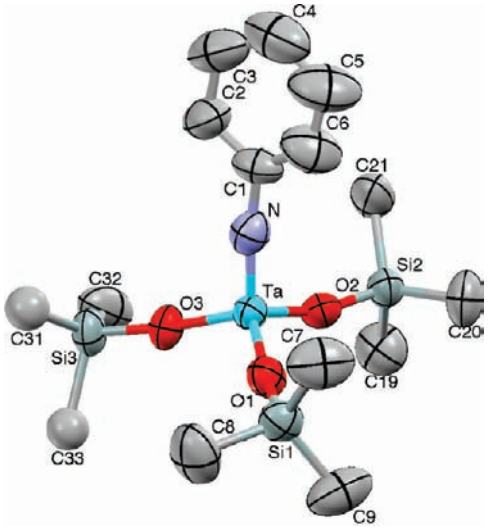

Figure 2. Molecular view of $(silox)_3Ta{=}NPh$ (**1**=NPh) with the peripheral Me groups removed for clarity. Selected distances (Å) and angles (deg): TaN, 1.767(10); TaO1, 1.894(7); TaO2, 1.891(7); TaO3, 1.893(6); SiO(ave), 1.663(11); NC1, 1.425(15); TaNC1, 172.4(8); NTaO1, 108.0(4); NTaO2, 105.9(5); NTaO3, 109.6(3); O1TaO2, 111.4(3); O1TaO3, 111.0(3); O2TaO3, 110.8(3); TaO1Si1, 169.2(5); TaO2Si2, 164.7(5); TaO3Si3, 172.9(5).

5. 1,2-H_2-Elimination from $(silox)_3HTaEHR$. An assessment of the mechanism of 1,2-H_2-elimination from $(silox)_3HTaEHR$ (**2**-EHR) was made via an evaluation of the rates as monitored by ^1H NMR spectroscopy in C_6D_6

(53) Drago, R. S. *J. Phys. Chem.* **1958**, *62*, 353–357.
(54) Power, P. P. *Chem. Rev.* **1999**, *99*, 3463–3503.
(55) Kutzelnigg, W. *Angew. Chem., Int. Ed. Engl.* **1984**, *23*, 272.
(56) Magnusson, E. *J. Am. Chem. Soc.* **1984**, *106*, 1177–1185.
(57) Nugent, W. A.; Mayer, J. M. *Metal-Ligand Multiple Bonds*; John Wiley & Sons: New York, 1988.

Table 3. Selected Crystallographic and Refinement Data for (silox)$_3$Ta=NPh (**1**=NPh), (silox)$_3$Ta=CPPh$_3$ (**1**=CPPh$_3$), [(silox)$_3$MeTa](μ-η^2-*N*,*N*:η^1-*C*-NHNHCH$_2$CH$_2$-CH$_2$)[Ta(κ-O,C-OSi^{t}Bu$_2$CMe$_2$CH$_2$)(silox)$_2$] (**7**), and [(silox)$_2$ClTa](μ-N$_2$) (**8**-Cl)

	1=NPh	**1**=CPPh$_3$	**7**	**8**-Cl
formula	$C_{42}H_{86}NO_3Si_3Ta$	$C_{55}H_{96}O_3PSi_3Ta$	$C_{76}H_{172}N_2O_6Si_6Ta_2$	$C_{48}H_{108}N_2O_4Cl_2Si_4Ta$
formula wt	918.34	1101.51	1740.60	1322.52
space group	$Pna2_1$	$P2_1/n$	$P\bar{1}$	$P2_1/c$
Z	4	4	2	4
a, Å	18.114(4)	11.8368(2)	12.7517(6)	14.6904(6)
b, Å	13.436(3)	22.2055(4)	17.5127(9)	27.0349(10)
c, Å	20.650(4)	22.1197(4)	23.2899(11)	17.4888(7)
α, deg	90	90	103.755(2)	90
β, deg	90	90.1200(10)	90.992(2)	113.637(2)
γ, deg	90	90	110.627(2)	90
V, Å^3	5025.8(19)	5813.97(18)	4698.7(4)	6363.0(4)
ρ_{calc}, g·cm^{-3}	1.214	1.258	1.230	1.381
μ, mm^{-1}	2.291	2.018	2.446	3.633
temp, K	293(2)	173(2)	173(2)	173(2)
λ (Å)	0.71073	0.71073	0.71073	0.71073
R indices [$I > 2\sigma(I)$][a,b]	R_1 = 0.0415	R_1 = 0.0404	R_1 = 0.0611	R_1 = 0.0566
	wR_2 = 0.0976	wR_2 = 0.0739	wR_2 = 0.1429	wR_2 = 0.1309
R indices (all data)[a,b]	R_1 = 0.0733	R_1 = 0.0674	R_1 = 0.0912	R_1 = 0.0980
	wR_2 = 0.1186	wR_2 = 0.0824	wR_2 = 0.1549	wR_2 = 0.1561
GOF[c]	1.080	1.028	1.059	1.014

[a] $R_1 = \sum||F_o| - |F_c||/\sum|F_o|$. [b] $wR_2 = [\sum w(|F_o| - |F_c|)^2/\sum wF_o^2]^{1/2}$. [c] *GOF* (all data) $= [\sum w(|F_o| - |F_c|)^2/(n-p)]^{1/2}$, n = number of independent reflections, p = number of parameters.

Table 4. Rate Constants[a,b] for 1,2-H$_2$-Elimination from (silox)$_3$HTaEHR (**2**-EHR), with and without Added H$_2$ER and Radical Trap C$_6$H$_8$ Obtained by ^{1}H NMR Spectroscopic Monitoring

cmpd	[HTaEHR]	[H$_2$ER]	[C_6H_8]	T(°C)	k ($\times 10^5$ s^{-1})
(silox)$_3$HTaNH$_2$ (**2**-NH$_2$)[c,d]	0.050			136.2(4)	166(5)
	0.056			119.0(4)	42.2(7)
	0.053			109.6(4)	18.8(4)
	0.053			99.1(4)	7.3(1)
	0.053			90.0(0)	2.73(2)
(silox)$_3$HTaNHMe (**2**-NHMe)	0.029			24.8(4)	2.49(6)
	0.029	0.363		24.8(4)	29.0(10)
	0.038[e]			24.8(4)	2.60(4)
(silox)$_3$HTaNPh (**2**-NHPh)[f]	0.060			24.8(4)	3.8(2)
	0.062	0.373		24.8(4)	3.8(2)
(silox)$_3$HTaNH(C$_6$H$_4$-*p*-Me) (**2**-NHC$_6$H$_4$-*p*-Me)	0.058[g]			24.8(4)	5.2(1)
(silox)$_3$HTaNH(C$_6$H$_4$-*p*-NMe$_2$) (**2**-NHC$_6$H$_4$-*p*-NMe$_2$)	0.033[h]			24.8(4)	22(1)
	0.053			24.8(4)	23.2(6)
(silox)$_3$DTaNH(C$_6$H$_4$-*p*-NMe$_2$) (**2D**-NHC$_6$H$_4$-*p*-NMe$_2$)	0.065[h,i]			24.8(4)	20.0(2)
(silox)$_3$HTaNH(C$_6$H$_4$-*p*-CF$_3$) (**2**-NHC$_6$H$_4$-*p*-CF$_3$)	0.062			24.8(4)	1.14(2)
(silox)$_3$DTaNH(C$_6$H$_4$-*p*-CF$_3$) (**2D**-NHC$_6$H$_4$-*p*-CF$_3$)[j]	0.062			24.8(4)	1.12(8)
(silox)$_3$HTaPH$_2$ (**2**-PH$_2$)[k,l]	0.034			24.8(4)	1.06(1)
	0.056			24.8(4)	1.04(7)
	0.060		0.060	24.8(4)	1.07(2)
(silox)$_3$HTaPHPh (**2**-PHPh)[m]	0.029[m]			24.8(4)	0.26(2)
	0.064[j]			24.8(4)	0.272(6)
	0.037[j]	0.109		24.8(4)	0.28(3)
	0.054[m]		0.054	24.8(4)	0.275(4)
(silox)$_3$HTaAsHPh (**2**-AsHPh)[n]	0.053			−76(1)	140(10)
	0.037		0.037	−9.5(10)	33(1)
	0.040		0.398	−9.5(10)	33(1)

[a] Determined from unweighted, non-linear, least-squares fitting of the exponential form of the rate expression (averaged where simultaneous runs were obtained); concentrations are in M. [b] **2**-NHR generated from **1** and RNH$_2$ unless otherwise indicated; monitored via disappearance of Ta*H*. [c] **2**-NH$_2$ isolated prior to runs. [d] $\Delta H^{\ddagger} = 25.3(8)$ kcal/mol; $\Delta S^{\ddagger} = -10(2)$ eu. [e] Monitored via loss of NH(C*H*$_3$). [f] Generated from **2**-H and RNH$_2$. [g] Monitored by disappearance of ArC*H*$_3$. [h] Monitored via the appearance of imido N(C*H*$_3$)$_2$. [i] Generated from (silox)$_3$TaD$_2$ (**2D**-D) and H$_2$NC$_6$H$_4$-*p*-NMe$_2$; run under ~1 atm D$_2$. [j] Generated from (silox)$_3$TaD$_2$ (**2D**-D) and H$_2$NC$_6$H$_4$-*p*-CF$_3$; monitored by disappearance of NH. [k] Isolated prior to run. [l] Monitored via appearance of P*H*. [m] Monitored via disappearance of Ta*H*. [n] **2**-EHR generated from **1** and H$_2$ER.

or C$_7$D$_8$. Table 4 lists rate constants obtained (typically an average of two or three runs) under various conditions. Rates were measured by generating **2**-EHR in situ when isolation of the pure compound was not possible. The eliminations were found to be first order in metal-hydride, and while the addition of H$_2$NMe was found to accelerate the elimination rate in the case of **2**-NHMe, the addition of PhNH$_2$ and PhPH$_2$ to **2**-NHPh and **2**-PHPh, respectively, failed to induce a change in the observed rates. It may be that only small bases have the ability to catalytically assist in the H-transfer, perhaps via the formation of (silox)$_3$Ta(EHR)$_2$ and H$_2$, and subsequent elimination of H$_2$ER. EH$_3$ could not be added to **2**-EH$_2$, since **3**-(EH$_2$)$_2$ was found to form for E = N, As. Trace amounts of EH$_2$R were common in NMR tube experiments where hydrolysis of Ta−EHR bonds can typically occur during

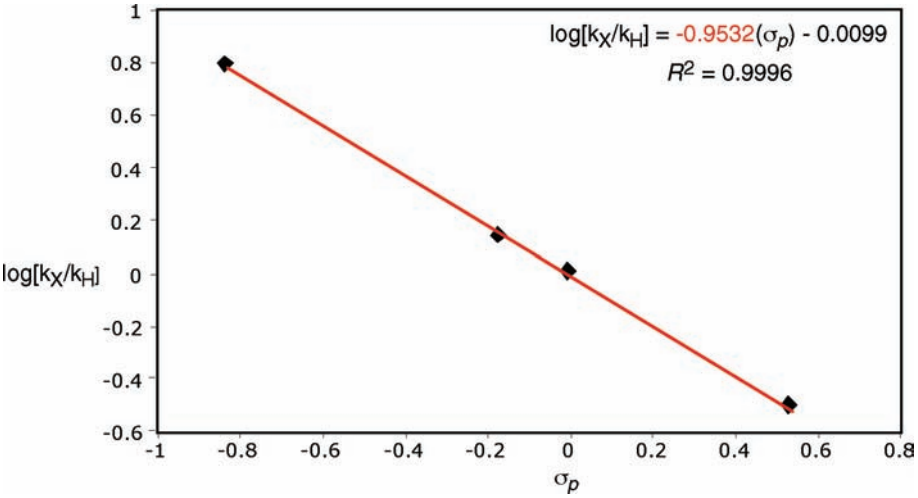

Figure 3. Hammett plot for 1,2-H_2-elimination from $(silox)_3HTa(NHC_6H_4$-*p*-X) (**2**-NHC_6H_4-*p*-X; X (σ_p) = NMe_2 (−0.83), CH_3 (−0.17), H (0.0), CF_3 (0.54)).

sealing of the tube. Fortunately, **2**-NH_2 and **2**-PH_2 could be isolated and purified prior to kinetics runs, no evidence of **3**-$(NH_2)_2$ and **3**-$(PH_2)_2$ was obtained during the runs, and the data for these substrates was reproducible. The results are thus interpreted as a straightforward 1,2-H_2-elimination, but with the caveat that trace base interference cannot be completely ruled out.[58]

Some of the rate data are readily interpreted, as the Hammett plot for 1,2-H_2-elimination from $(silox)_3HTa(NHC_6H_4$-*p*-X) (**2**-NHC_6H_4-*p*-X) in Figure 3 exemplifies. Its slope of −0.95 suggests a stabilization of positive charge at nitrogen in the transition state, perhaps an indication that greater N→Ta donation increases the rate of reaction through both π- (*p*-NMe_2) and σ-donation (*p*-Me). A temperature dependent study (90.0(4)−136.2(4)°C) of 1,2-H_2-elimination from $(silox)_3HTaNH_2$ (**2**-NH_2) afforded Eyring parameters of $\Delta H^{\ddagger}$ = 25.3(8) kcal/mol and $\Delta S^{\ddagger}$ = −10(2) eu.[59−61] The parameters permit the 1,2-H_2-elimination rate for **2**-NH_2 to be calculated at 24.8 °C as 1.11×10^{-8} s^{-1}, thus the relative rates for **2**-NHR are R = Ph (3420), Me (2340), and H (1). It appears that the π-system of Ph and the σ-donor ability of Me speed up the elimination, and these relative rates are significantly faster than H. The trend is consistent with the expectedly weaker *D*(NH) for the pseudobenzylic -NHPh group (*D*(NH) = 92 kcal/mol in H_2NPh)[62] versus the −NHMe (*D*(NH) = 100 kcal/mol in H_2NMe) and -NH_2 (*D*(NH) = 107 kcal/mol in NH_3)[63] fragments, suggesting that the transition state is early, which is typical for an irreversible process. The trend also parallels pK_a's of the corresponding aniline (30.6),[62] methylamine (∼38−40), and ammonia (41), although the disparity between the Me and H substituents in **2**-NHR relative to Ph is greater than predicted. The k_H/k_D's of 1.10(6) (i.e., k(**2**-$NHC_6H_4NMe_2$)/k(**2D**-$NHC_6H_4NMe_2$)) and 1.02(10) (i.e., k(**2**-$NHC_6H_4CF_3$)/k(**2D**-$NHC_6H_4CF_3$)) are not significant,[64] since the hydrogen being transferred is the one attached to N. No scrambling between hydride and amide sites were observed. Unfortunately, measurements of the complementary KIE for k(**2**-NHC_6H_4-NMe_2)/k(**2**-$NDC_6H_4NMe_2$) were not conducted because it proved difficult to prepare **2**-$NDC_6H_4NMe_2$ in sufficient isotopic purity.

A separate problem was revealed upon reproduction of data pertaining to the 1,2-H_2-elimination from $(silox)_3$-HTaAsHPh (**2**-AsHPh). While an elimination rate of $1.4(1) \times 10^{-3}$ s^{-1} was obtained at −76 °C, it was subsequently found that this was due to processes that were shut down via the addition of 1,4-cyclohexadiene, a common radical trap. If $\Delta S^{\ddagger}$ for H_2 elimination from **2**-AsHPh is also −10 eu, then its rate can be estimated at 24.8 °C to be $\sim 2.0 \times 10^{-4}$ s^{-1}, and the relative 1,2-H_2-elimination rates from $(silox)_3HTaEHPh$ (**2**-EHPh) are As (5800) > N (14) > P (1).

Attempts to Synthesize [(silox)$_3$Ta](μ-N_2). 1. 1,2-H_2-Elimination and Aziridine Strategies. As Scheme 2 implies, the oxidative addition of a substrate such as hydrazine, H_2N-NH_2, was envisaged to undergo 1,2-NH-additions to sequential $(silox)_3Ta$ (**1**) centers in concert with 1,2-H_2-eliminations to afford the desired N_2 complex, $[(silox)_3$-$Ta]_2(\mu$-$N_2)$ (**1**$_2$-N_2). Unfortunately, elimination of NH_3 instead of H_2 occurred independent of stoichiometry, yielding $(silox)_3Ta$=NH (**1**=NH, eq 1).[65] Negligible amounts of

$$\underset{\mathbf{1}}{(silox)_3Ta} + H_2N\text{-}NH_2 \xrightarrow[23^\circ C]{C_6D_6} \underset{\mathbf{2}=NH}{(silox)_3Ta{=}NH} + NH_3 \quad (1)$$

$$\underset{\mathbf{1}}{(silox)_3Ta} + H_2N\text{-}N(^cNC_2H_3Me) \xrightarrow[23^\circ C]{C_6D_6} \underset{\mathbf{2}=NH}{(silox)_3Ta{=}NH} + H^cNC_2H_3Me \quad (2)$$

1=NH(NH_3) and $(silox)_3Ta(NH_2)_2$ (**3**-$(NH_2)_2$) were observed, as expected for the low concentration of product

(58) Baratta, W.; Siega, K.; Rigo, P. *Chem.—Eur. J.* **2007**, *13*, 7479–7486.
(59) Bennett, J. L.; Wolczanski, P. T. *J. Am. Chem. Soc.* **1997**, *119*, 10696–10719.
(60) Schaller, C. P.; Cummins, C. C.; Wolczanski, P. T. *J. Am. Chem. Soc.* **1996**, *118*, 591–611.
(61) Schaller, C. P.; Wolczanski, P. T. *Inorg. Chem.* **1993**, *32*, 131–144.
(62) Bordwell, F. G.; Zhang, X.-M.; Cheng, J.-P. *J. Org. Chem.* **1993**, *58*, 6410–6416.
(63) McMillen, D. F.; Golden, D. M. *Annu. Rev. Phys. Chem.* **1982**, *33*, 493–532.
(64) Carpenter, B. K. *Determination of Reaction Mechanisms*; Wiley-Interscience: New York, 1984.
(65) Shaver, M. P.; Fryzuk, M. D. *J. Am. Chem. Soc.* **2005**, *127*, 500–501.

Scheme 3

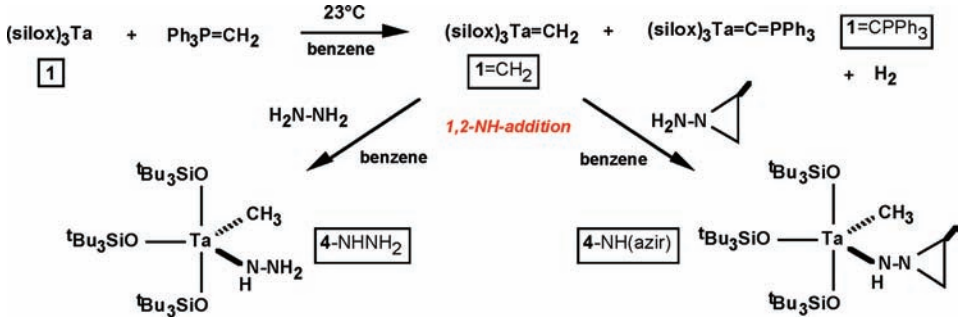

NH_3. It appears that 1,2-H_2-elimination from putative $(silox)_3HTaNH(NH_2)$ (**2**-$NHNH_2$) is simply uncompetitive with respect to 1,2-HN-elimination, although N−N oxidative addition followed by NH_3 loss cannot be excluded. A related approach, utilizing the addition of *N*-amino-2-methylaziridine,[66] was considered in the hope that propene loss and formation of $(silox)_3Ta{=}N\text{-}NH_2$ (**1**=NNH_2) would permit a stepwise synthesis of $\mathbf{1}_2$-N_2. Unfortunately, $(silox)_3Ta{=}NH$ (**1**=NH) was the product, consistent with 2-methylaziridine loss analogous to that delineated for hydrazine (eq 2); byproducts (e.g., $(silox)_3Ta(\eta\text{-}C_2H_3Me)$ as in Scheme 2) were consistent with the reaction of 2-methylaziridine (shown as the initial product in eq 2) with **1**.

2. Synthesis of $(silox)_3Ta{=}CH_2$. In an attempt to obviate the presumed deleterious, swift 1,2-HN-elimination reaction, routes to $(silox)_3RTaNHNH_2$ and $(silox)_3$-RTaNH(2-Me-aziridine) were sought in the hope that 1,2-RH-elimination to give the desired imides would be controllable. As Scheme 3 illustrates, successful implementation of this route required the preparation of $(silox)_3Ta{=}CH_2$ (**1**=CH_2),[26] which was accomplished via methylene transfer to $(silox)_3Ta$ (**1**) from $Ph_3P{=}CH_2$;[67] related attempts with Me_3PCH_2,[68] which would yield the easily removable PMe_3 as a byproduct, afforded complex mixtures. As is typical for reactions with the Wittig reagent, removal of byproduct Ph_3P was difficult, but a 29% yield of **1**=CH_2 was obtained after multiple crystallizations from hexane. During the course of optimizing the synthesis, a curious byproduct was obtained that was devoid of hydrogens other than those of phenyl or silox. The compound, which could be isolated in 20% yield, possessed a single $^{31}P\{^1H\}$ NMR spectral shift at δ −4.26 and a unique $^{13}C\{^1H\}$ NMR spectral resonance at δ 175.01 that appeared as a doublet with J_{PC} = 53 Hz, consistent with the formulation $(silox)_3Ta{=}C{=}PPh_3$ (**1**=$CPPh_3$). Its structure was confirmed by X-ray crystallography.

3. Structure of $(silox)_3Ta{=}C{=}PPh_3$. Selected crystallographic details of $(silox)_3Ta{=}C{=}PPh_3$ (**1**=$CPPh_3$) are given in Table 3, and Figure 4 illustrates its near C_{3v} core configuration, with the silox groups staggered relative to the phosphine phenyl substituents on the periphery. The Ta−C−P linkage is virtually linear (177.83(17)°), and the *d*(TaC) is quite short at 1.862(2) Å, signifying substantial

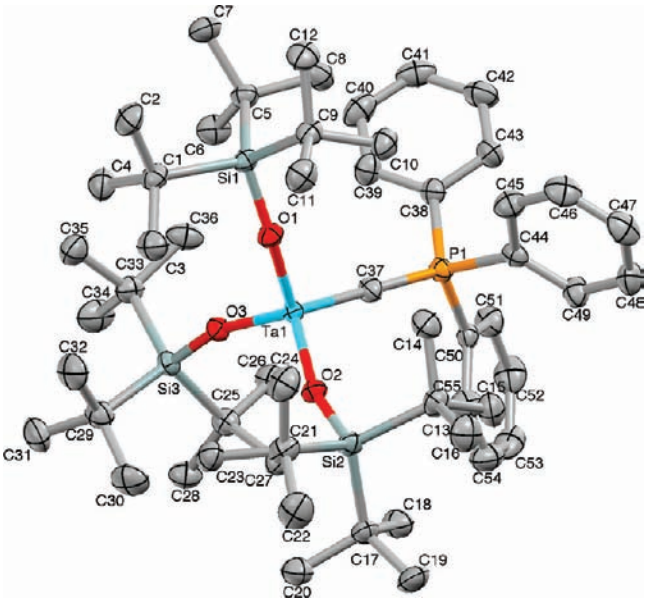

Figure 4. Molecular view of $(silox)_3Ta{=}C{=}PPh_3$ (**1**=$CPPh_3$). Selected distances (Å) and angles (deg): Ta−C37, 1.862(2); Ta−O1, 1.9122(16); Ta−O2, 1.9072(15); Ta−O3, 1.9139; P−C37, 1.667(2); P−C^{Ph}(ave), 1.816(3); Si−O(ave), 1.655(5); Ta−C37−P, 177.83(17); O1−Ta−C37, 109.24(9); O2−Ta−C37, 108.66(9); O3−Ta−C37, 108.27(9); O1−Ta−O2, 110.45(7); O1−Ta−O3, 108.81(7); O2−Ta−O3, 111.36(7); C37−P−C^{Ph}(ave), 113.7(7); C^{Ph}−P−C^{Ph}(ave), 105.0(7); Ta−O−Si(ave), 163.6(19).

triple bond character.[59] The accompanying PC distance of 1.667(2) Å is slightly shorter than expected for a P−C(sp) single bond (1.78 Å), consistent with considerable double bond character; hence, the unit can be construed as having contributions from both Ta=C=P and $Ta^{(-)}{\equiv}C{-}P^{(+)}$ resonance structures. Similar constructs have been useful in rationalizing phosphacarbene/yne groups in related molecules.[69−72] The remainder of the core has standard $(silox)_3Ta^V$ parameters that are given in the caption to Figure 3.

(66) Hillers, S.; Eremeev, A. V.; Lidaks, M.; Pestunovich, V. A.; Liepin, E.; Kalvins, I. *Khim. Geterotsikl. Soedin.* **1971**, *7*, 45–48.
(67) Sharp, P. R.; Schrock, R. R. *J. Organomet. Chem.* **1979**, *171*, 43–51.
(68) Klein, H. F. *Inorg. Synth.* **1978**, *18*, 139.
(69) (a) Jamison, G. M.; White, P. S.; Templeton, J. L. *Organometallics* **1991**, *10*, 1954–1959. (b) Bruce, A. E.; Gamble, A. S.; Tonker, T. L.; Templeton, J. L. *Organometallics* **1987**, *6*, 1350–1352.
(70) List, A. K.; Hillhouse, G. L.; Rheingold, A. L. *Organometallics* **1989**, *8*, 2010–2016.
(71) (a) Li, X. Y.; Wang, A.; Wang, L.; Sun, H.; Harms, K.; Sundermeyer, J. *Organometallics* **2007**, *26*, 1411–1413. (b) Li, X. Y.; Sun, H. J.; Harms, M.; Sundermeyer, J. *Organometallics* **2005**, *19*, 4699–4701. (c) Li, X. Y.; Schopf, M.; Stephan, J.; Harms, M.; Sundermeyer, J. *Organometallics* **2002**, *21*, 2356–2358.
(72) Cordiner, R. L.; Gugger, P. A.; Hill, A. F.; Willis, A. C. *Organometallics* **2009**, *28*, 6632–6635.

Scheme 4

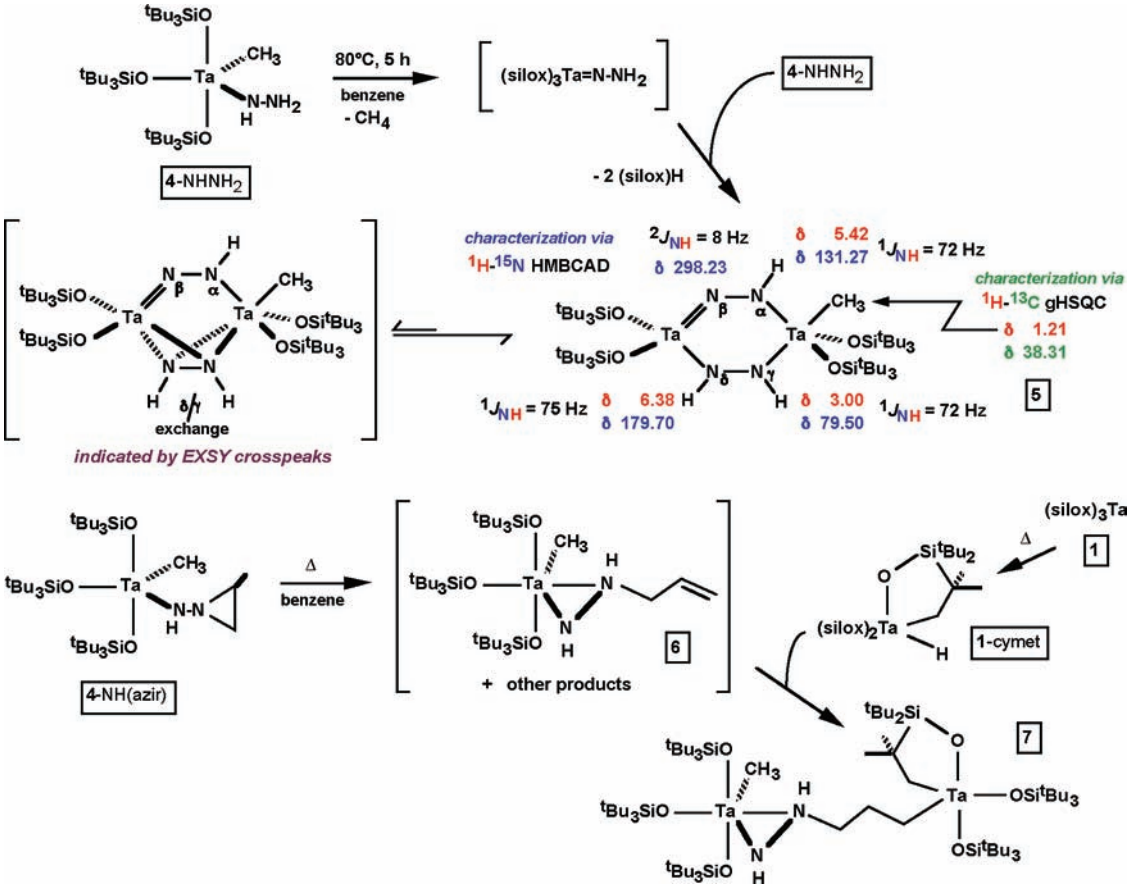

4. 1,2-RH-Elimination Attempts. As Scheme 3 reveals, the addition of hydrazine to $(silox)_3Ta{=}CH_2$ (**1**$=CH_2$) afforded $(silox)_3MeTaNHNH2$ (**4**-$NHNH_2$) in 70% yield. Although **4**-$NHNH_2$ was modestly thermally sensitive, NMR spectral characterization was readily accomplished using $^1H-^{15}N$ HSQCAD correlation spectroscopy.[73] In addition to the silox and Me proton resonances, different nitrogens at δ 64.80 and δ 148.47 (J_{NH} = 78 Hz) were observed to correspond with proton signals at δ 3.63 and δ 4.11, and these were assigned to the NH_2 and NH groups, respectively. Similarly, treatment of **1**$=CH_2$ with amino-2-methylaziridine provided $(silox)_3MeTaNH$-(-^{c}NCHMeCH$_2$) (**4**-NH(azir)) in 60% yield as a waxy solid. The aziridine nitrogen was indirectly found at δ 81.99 (^{15}N), and the accompanying NH was located at δ 244.46 with J_{NH} = 72 Hz. Subsequent thermolyses of the methyl-hydrazides generated derivatives that proved to be more complicated than those expected from simple 1,2-MeH-eliminations.

Thermal degradation of $(silox)_3MeTaNHNH2$ (**4**-$NHNH_2$) led to the loss of MeH, but evidence of (silox)H was also obtained, and NMR spectroscopic data were more consistent with a dinuclear species with four inequivalent silox groups. Attempts to rid the solutions of byproduct (silox)H invariably led to further degradation, thus it is conceivable that the silanol is weakly hydrogen-bonded to the product, especially when solutions are concentrated. Successful implementation of $^1H-^{15}N$ HMBCAD NMR correlation spectroscopy enabled the connectivity of the N-containing bridges to be ascertained, and an elusive Me group, partially masked by the silox resonances, was brought to light by $^1H-^{13}C$ gHSQC NMR correlation spectroscopy.[74] The product is thought to be $[(silox)_2TaMe](\mu\text{-}N_\alpha HN_\beta)(\mu\text{-}N_\gamma HN_\delta H)[Ta(silox)_2]$ (**5**), which is portrayed in Scheme 4. Attempts to crystallize **5** in the presence of (silox)H led to waxy solids of reasonable purity, but these were not amenable to X-ray diffraction analysis. As such, the hapticity and orientation of bridges and silox groups are undetermined. Nonetheless, the NMR spectroscopy clearly shows a diamido μ-NH-NH bridge accompanied by an imido-amide μ-NH-N unit. The shift of one amide ($N_\gamma H$, δ 79.50) is substantially lower than the remaining two ($N_\alpha H$, δ 131.27; $N_\delta H$, δ 179.70), and may be indicative of a strong σ-donor (i.e., Me) opposite it in the complex. The imido nitrogen is observed more downfield at δ 298.23. EXSY correlation spectroscopy revealed exchange between $N_\gamma H$ and $N_\delta H$, thus it is possible that this bridge exists as an $\eta^2,\eta^{2/1}$-NH, NH unit[12,75,76] or this configuration is at least energetically feasible to permit rapid exchange, as Scheme 4 shows.

(73) Koshino, H.; Uzawa, J. *Kagaku Seibutsu* **1995**, *33*, 252–258.

(74) Friebolin, H. *Basic One- and Two-Dimensional NMR Spectroscopy*; Wiley-VCH: Weinheim, 2005.

(75) Fryzuk, M. D.; Love, J. B.; Rettig, S. J.; Young, V. G. *Science* **1997**, *275*, 1445–1447.

(76) Bernskoetter, W. H.; Pool, J. A.; Lobkovsky, E.; Chirik, P. J. *J. Am. Chem. Soc.* **2005**, *127*, 7901–7911.

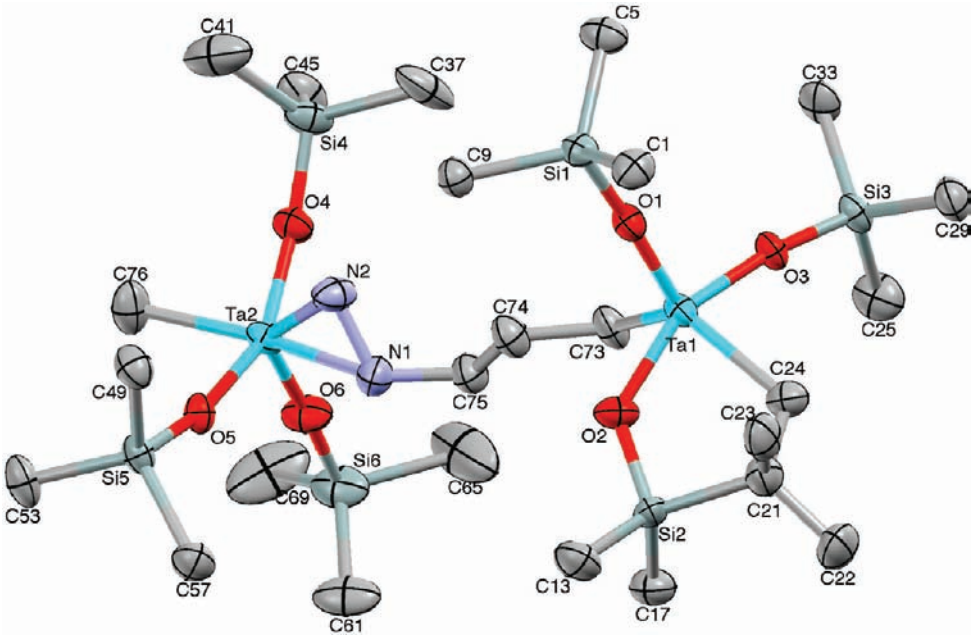

Figure 5. Molecular view of [(silox)$_3$MeTa](μ-η^2-*N*,*N*:η^1-*C*-NHNHCH$_2$CH$_2$CH$_2$)[Ta(κ-O,C-OSi^{t}Bu$_2$CMe$_2$CH$_2$) (silox)$_2$] (**7**) with the methyls of the ^{t}Bu groups removed for clarity. Selected distances (Å) and angles (deg): Ta1−O1, 1.862(8); Ta1−O2, 1.932(5); Ta1−O3, 1.905(5); Ta1−C24, 2.217(9); Ta1−C73, 2.133(8); C73−C74, 1.523(11); C74−C75, 1.481(12); N1−C75, 1.441(11); N1−N2, 1.384(11); Ta2−N1, 2.283(7); Ta2−N2, 2.008(7); Ta2−C76, 2.211(9); Ta2−O4, 1.915(5); Ta2−O5, 1.951(5); Ta2−O6, 1.896(6); Si−O(ave), 1.662(11); O1−Ta1−O2, 100.4(2); O1−Ta1−O3, 104.8(2); O2−Ta1−O3, 154.6(2); O1−Ta1−C24, 123.8(3); O1−Ta1−C73, 111.0(3); O2−Ta1−C24, 77.0(3); O2−Ta1−C73, 86.0(3); O3−Ta1−C24, 86.1(3); O3−Ta1−C73, 88.3(3); O4−Ta2−N1, 108.7(3); O4−Ta2−N2, 85.0(3); O4−Ta2−O5, 152.7(2); O4−Ta2−O6, 100.4(2); O4−Ta2−C76, 83.1(3); O5−Ta2−N1, 79.4(2); O5−Ta2−N2, 87.4(3); O5−Ta2−O6, 105.3(2); O5−Ta2−C76, 82.8(3); O6−Ta2−N1, 93.1(3); O6−Ta2−N2, 126.0(3); O6−Ta2−C76, 101.3(3); N1−Ta2−N2, 36.9(3); N1−Ta2−C76, 159.6(3); N2−Ta2−C76, 132.6(3); Ta1−C73−C74, 118.2(6); C73−C74−C75, 114.5(8); C74−C75−N1, 115.8(8); N2−N1−C75, 114.7(7); N1−N2−Ta2, 82.4(4); Ta2−N1−C75, 136.8(6); Ta2−N1−N2, 60.7(4); Ta1−O2−Si2, 131.5(4); O2−Si2−C21, 96.4(4); Si2−C21−C24, 102.7(6); Ta1−C24−C21, 119.7(6).

The failure to generate (silox)$_3$Ta=NNH$_2$ as a stable entity[77,78] prompted a turn toward the aziridine chemistry, and (silox)$_3$MeTaNH(-^{c}NCHMeCH$_2$) (**4**-NH(azir)) was treated with 2 equiv of (silox)$_3$Ta (**1**) with the hope of producing (silox)$_3$MeTaNH-N=Ta(silox)$_3$ and (silox)$_3$Ta(η-C$_3$H$_6$). Unfortunately, no deolefination of the aziridine was noted at 23 °C, and thermolysis **4**-NH(azir) under varied conditions could not be accomplished without significant cyclometalation of **1** to give (silox)$_2$HTa(κ-O,C-OSi^{t}Bu$_2$CMe$_2$CH$_2$) (**1**-cymet).[6,15] During the thermolysis, several products were noted, including those containing olefinic residues, consistent with ring-opening of the aziridine[79] to (silox)$_3$MeTaNHNH-CH$_2$CH=CH$_2$ (**6**). Yellow crystals that proved to be nearly insoluble in common hydrocarbons were observed to form during this process, and X-ray crystallographic studies revealed this material to be [(silox)$_3$MeTa](μ-η^2-*N*,*N*:η^1-*C*-NHNHCH$_2$CH$_2$CH$_2$)[Ta(κ-O,C-OSi^{t}Bu$_2$CMe$_2$-CH$_2$)(silox)$_2$] (**7**). As Scheme 4 illustrates, **7** is best thought of arising from insertion of the olefin of **6** into the Ta−H bond of **1**-cymet.[15]

The treatment of (silox)$_3$Ta=CH$_2$ (**1**=CH$_2$) with diimines was also considered in view of Schrock's preparation of [(THF)$_2$Cl$_3$Ta]$_2$(μ-N$_2$).[9] Unfortunately, stable diimines such as PhCH=N−N=CHPh failed to react with the methylene derivative, presumably because of deleterious steric interactions in the putative 4-membered ring intermediate.

6. Structure of [(silox)$_3$MeTa](μ-η^2-*N*,*N*:η^1-C-NH-NHCH$_2$CH$_2$CH$_2$)[Ta(κ-O,C-OSi^{t}Bu$_2$CMe$_2$CH$_2$) (silox)$_2$] (7). With solubility precluding a definitive NMR analysis of [(silox)$_3$MeTa](μ-η^2-*N*,*N*:η^1-CNHNHCH$_2$CH$_2$CH$_2$)-[Ta(κ-O,C-OSi^{t}Bu$_2$CMe$_2$CH$_2$)(silox)$_2$] (**7**), an X-ray crystallographic study (Table 3) was conducted on the aforementioned yellow crystals. Despite one badly disordered set of silox ^{t}Bu groups (on Si6), the study yielded a reasonable model that illustrates the ring-opened aziridine product as illustrated by Figure 5. The cyclometalated center is fairly well described as a pseudo-tbp geometry with the two less-electronegative alkyl substituents in their expected equatorial positions.[3,80] The chain linkage, Ta1−C73, is 2.133(8) Å, and the cyclometalated *d*(Ta1−C24) is 2.217(9) Å, and both are separated by 124.5(4)°. The remaining pseudo-equatorial position is occupied by O1, which is 1.862(5) Å from the tantalum, and 111.0(3)° and 123.8(3)° from C73 and C24, respectively. Siloxide oxygens O2 and O3 are 1.932(5) and 1.905(5) Å from the tantalum, respectively, which are slightly longer than O1 and consistent with their pseudoaxial positions. The bite angle of the cylometalated silox is 77.0(3)°, and its oxygen, O2, is 100.4(2)° and 86.0(3)° from O1 and C73, respectively.

One can similarly assess the hydrazide-methyl core, taking TaO4 (1.915(5) Å) and TaO5 (1.951(5) Å) as pseudoaxial siloxides (∠O4−Ta2−O5 = 152.7(2)°), and Ta2O6 (1.896(6) Å) as a pseudo-equatorial siloxide, 100.4(2)° and 105.3(2)° from O4 and O5, respectively.

(77) Sebe, E.; Heeg, M. J.; Winter, C. H. *Polyhedron* **2006**, *25*, 2109.
(78) Tonks, I. A.; Bercaw, J. E. *Inorg. Chem.* **2010**, *49*, 4648–4656.
(79) Kashelikar, D. V.; Fanta, P. E. *J. Org. Chem.* **1961**, *26*, 1841–1842.
(80) Strazisar, S. A.; Wolczanski, P. T. *J. Am. Chem. Soc.* **2001**, *123*, 4728–4740.

Scheme 5

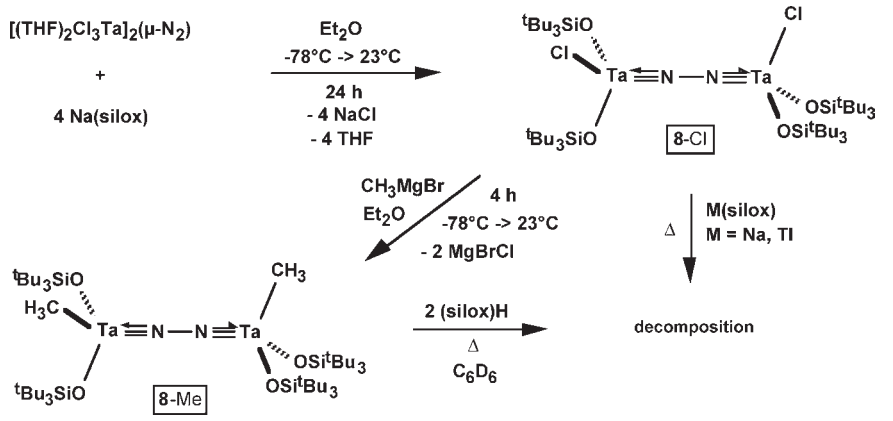

This assessment treats the NH-NHR ligand as occupying one site. The methyl is pseudo-equatorial (2.211(9) Å) along with the amide of the hydrazide (d(Ta2−N2) = 2.008(7) Å; d(N1−N2) = 1.384(11) Å), and the trans influence of the donor nitrogen, N2 (2.283(7), ∠C76−Ta2−N1 = 159.6(3)°), helps slightly weaken the methyl interaction. The remaining core distances and angles are listed in the Figure 5 caption. Distances and angles pertaining to the bridge are consistent with a $(CH_2)_3$-NHNH linkage derived from ring-opening of the aziridene and trapping of the subsequent olefin by the hydride of the **1**-cymet, just as Scheme 4 portrays.

7. Attempted Oxidative Coupling of (silox)$_3$TaNLi. Conceptually, oxidation of the nitride anion, $(silox)_3$-TaNLi (**1**=NLi), can lead to the desired N_2-complex, but one electron oxidants invariably generated $(silox)_3$-Ta=NH (**1**=NH), presumably via H-atom abstraction by an incipient $(silox)_3TaN\cdot$ species. A more probable strategy would rely on N−N oxidative coupling induced by reductive elimination from $L_nM(NTa(silox)_3)_2$, as eq 3 implicates. Utilization of $(Ph_3P)_2PtCl_2$, $(Et_3P)_2PdCl_2$, $(DME)NiCl_2$, and other related complexes failed to induce N−N bond formation, and no evidence for M-N intermediates was found. Only for Cp_2TiCl_2 was NMR spectroscopic evidence for Cp_2ClTi-N=Ta$(silox)_3$ obtained, and its thermolysis yielded **1**=NH and Cp_2TiCl. Attempts to oxidatively add the NH bond of **1**=NH to $(Ph_3P)_4Pd$ and trap the product hydride with olefin also failed to provide any evidence of $(Ph_3P)_nPdH$(N=Ta-$(silox)_3$).

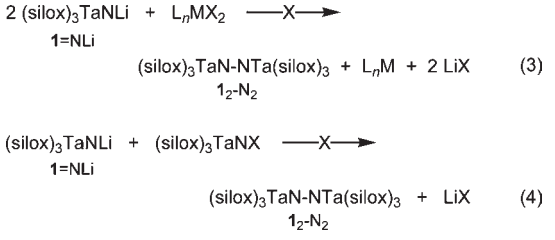

A potentially simpler route would require conversion of the anionic nitride into an electrophile of the type $(silox)_3$Ta=NX (**1**=NX), which would then be susceptible to attack by nitride $(silox)_3$TaNLi (**1**=NLi), as indicated by eq 4.[81] Unfortunately, attempts to halogenate the nitride anion with Br_2, I_2, or NBS failed to elicit any tractable material under a variety of conditions. Since $(silox)_3$Ta=NH was a common product in virtually all of the attempts, it appears that $1e^-$ reactivity is at the core of the problem.

Compromise, [(silox)$_2$ClTa](μ-N$_2$). 1. Synthesis of [(silox)$_2$ClTa](μ-N$_2$). Although a number of variants on the preceding methods are plausible, Schrock's diimide complexes, in particular $[(THF)_2Cl_3Ta]_2(\mu\text{-}N_2)$,[9] were considered as starting materials for metathesis reactions to attain some measure of success in a reasonable period of time. As Scheme 5 illustrates, treatment of the chlorodiimide derivative with 4 equiv of Na(silox) afforded $[(silox)_2ClTa](\mu\text{-}N_2)$ (**8**-Cl) is 56% yield. Further metathesis with Na(silox) or Tl(silox) on **8**-Cl failed to provide the desired $[(silox)_3Ta]_2(\mu\text{-}N_2)$ ($\mathbf{1}_2$-N_2) complex, and thermolysis ultimately led to degradation. Prior work[4] suggested that smaller siloxides/alkoxides would not support a 3-coordinate tantalum center. The chloride was converted to the Me derivative, $[(silox)_2MeTa](\mu\text{-}N_2)$ (**8**-Me, 70%) with MeMgBr, but subsequent attempts at silanolysis reactions with (silox)H did not generate MeH, and heating again led to decomposition. NMR spectra of **8**-Cl and **8**-Me revealed one type of silox, consistent with either C_{2h} symmetry and/or free rotation about the bridge.

2. Structure of [(silox)$_2$ClTa]$_2$(μ-N$_2$). Table 3 lists pertinent crystallographic information pertaining to the structure of $[(silox)_2ClTa]_2(\mu\text{-}N_2)$ (**8**-Cl), and Figure 4 provides two views of the molecule. Unfortunately, while the data confirm the C_2 structure, the electron density between the two heavy tantalum atoms would not yield a reliable solution; using an isotropic model for the bridging nitrogens, TaN distances of 1.780(7) and 1.739(8) Å, and a d(NN) of 1.355(11) Å were found, but these should not be construed as accurately portraying the bridge. Nonetheless, the conformation of **8**-Cl was confirmed, including a pseudo-eclipsed placement of the core substituents relative to the adjacent tantalum, as previously seen in $[(silox)_2XM]_2$ systems.[82] This arrangement essentially minimizes steric interactions across the bridge by

(81) Figueroa, J. S.; Piro, N. A.; Clough, C. R.; Cummins, C. C. *J. Am. Chem. Soc.* **2006**, *128*, 940–950.

(82) Miller, R. L.; Lawler, K. A.; Bennett, J. L.; Wolczanski, P. T. *Inorg. Chem.* **1996**, *35*, 3242–3253.

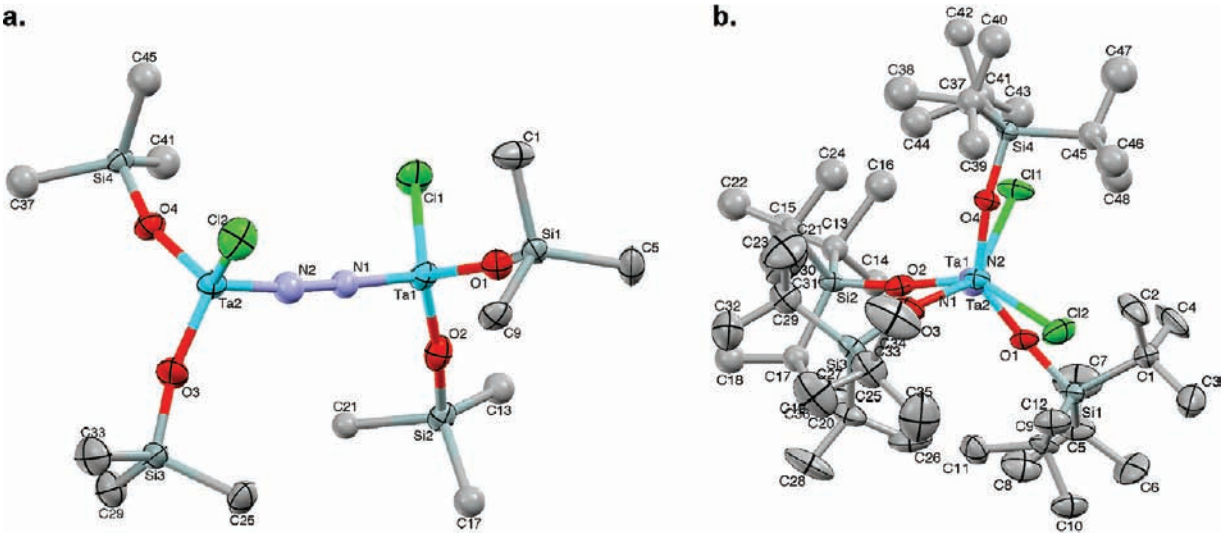

Figure 6. (a) Molecular view of $[(silox)_2ClTa]_2(\mu\text{-}N_2)$ (**8**-Cl) with peripheral Me groups removed for clarity; note the N atoms refined isotropically; see text for comments pertaining to the TaNNTa bridge. (b) End on view of **8**-Cl revealing typical C_2 symmetry of dimeric species. Selected distances (Å) and angles (deg): Ta1−O1, 1.869(6); Ta1−O2, 1.871(7); Ta2−O3, 1.868(7); Ta2−O4, 1.854(6); Ta1−Cl1, 2.312(2); Ta2−Cl2, 2.307(3); Si−O(ave), 1.652(5); N1−Ta1−O1, 109.2(3); N1−Ta1−O2, 111.4(3); N1−Ta1−Cl1, 107.5(3); O1−Ta1−O2, 110.7(3); O1−Ta1−Cl1, 109.5(2); O2−Ta1−Cl1, 108.5(2); N2−Ta2−O3, 111.6(4); N2−Ta2−O4, 108.5(3); N2−Ta2−Cl2, 107.9(3); O3−Ta2−O4, 109.6(3); O3−Ta2−Cl2, 109.8(2); O4−Ta2−Cl2, 109.5(2).

trading two minimal silox/Cl interactions for one significant silox/silox interaction. Only one type of silox group is observed in NMR spectra of **8**-Cl or $[(silox)_2\text{-}MeTa]_2(\mu\text{-}N_2)$ (**8**-Me), presumably because of rapid rotation about the TaNNTa linkage. Distances and angles of the pseudo-tetrahedral cores (109.5(13)°) are listed in Figure 6.

Discussion

Pnictogen Chemistry. 1. H_2ER Oxidative Addition to $(silox)_3Ta$. A previous study that employed substituents on $H_2N(C_6H_4\text{-}X)$ (X, k_{rel}: 3-CF_3, 0.30(7); 3-F, 0.63(12); 4-F, 0.89(17); H, 1; 4-Ph, 0.93(17); 4-Me, 1.2(2); 4-OMe, 1.9(2); 4-NMe_2, 2.5(2)) examined the relative rates (aniline at $k_{rel} = 1$) of NH oxidative addition via competition experiments.[3] As the basicity of the aniline increased ($\rho = -0.69$, $R = 0.93$), the relative rate of oxidative addition increased, consistent with nucleophilic attack by the amine at a vacant d_{xz}/d_{yz} orbital preceding oxidative addition. The correlation was modest, and separate Hammett parameters were indicative of slightly greater resonance than inductive contributions. While complementary studies of REH_2 oxidative addition to $(silox)_3Ta$ (**1**) were not examined, they qualitatively correlated with basicity of the substrate modified by steric factors.

2. 1,2-Dihydrogen-Elimination from (silox)HTaNHR. The 1,2-dihydrogen elimination data listed in Table 4 represent a limited, but reasonably interpretable set with regard to $(silox)_3HTaNHR$ (**2**-NHR). The activation parameters ($\Delta H^{\ddagger} = 25.3(8)$ and $\Delta S^{\ddagger} = -10(2)$ eu) for H_2 elimination from $(silox)_3HTaNH_2$ (**2**-NH_2) are fully consistent with previous 1,2-RH-eliminations of RH $(silox)_n(^tBu_3SiNH)_{3-n}MR$ species, whose $\Delta S^{\ddagger}$ values were typically −12 to −13 eu.[59−61] Since H does not need to reorganize prior to elimination, in contrast to R, the slightly less negative activation entropy observed is expected. Loss of RH/D from $(silox)_2(^tBu_3SiNH/D)TiR$ results in KIEs ranging from ∼7−15 at 24.8 °C,[59] and while the related experiments were not conducted in this study, the absence of a significant isotope effect in 1,2-HD-elimination from $(silox)_3DTaNH(C_6H_4\text{-}p\text{-}X)$ (**2D**-$NHC_6H_4\text{-}p\text{-}X$; X = CF_3, NMe_2) suggests that the activation is primarily one involving N−H breakage.

The Hammett study of 1,2-H_2-elimination from $(silox)_3$-$HTa(NHC_6H_4\text{-}p\text{-}X)$ (**2**-$NHC_6H_4\text{-}p\text{-}X$) in Figure 3, the relative rates of dihydrogen loss from $(silox)_3HTa$-(NHR) (**2**-NHR; R = Ph (3420), Me (2340), and H (1)), and the modest correlation with pK_a's of the corresponding amines support the contention that positive charge on N develops in the transition state. In **2**-NHR, N→Ta π-bonding also justifies the acidic character of the NH hydrogen, while the electropositive nature of tantalum relative to hydrogen ensures that the TaH bond is $Ta(\delta^+)-H(\delta^-)$. Two additional factors suggest that N−H bond breaking, viewed as having a $(NH)\delta^+$ component and hence having some proton transfer character, is the major bond activation. First, virtually no isotope effect is observed in the hydride position, as assessed via k(**2**-$NHC_6H_4\text{-}p\text{-}X$)/$k$(**2D**-$NHC_6H_4\text{-}p\text{-}X$)) (X = NMe_2, KIE = 1.10(6); CF_3, KIE = 1.02(10)). Second, a modest inverse correlation of rate versus D(H-NHR) is observed, where the weaker the bond, the faster the 1,2-H_2-elimination.

3. 1,2-H_2-Elimination from $(silox)_3HTaEHR$. While dihydrogen elimination from the nitrogen-containing species was reasonably explained, and consistent with the widely held view of charge distribution in early metal complexes, inclusion of phosphorus and arsenic muddies the waters. To reiterate, if $\Delta S^{\ddagger}$ for H_2 elimination from **2**-AsHPh is assumed to be −10 eu, the relative 1,2-H_2-elimination rates from $(silox)_3HTaEHPh$ (**2**-EHPh) at 24.8 °C are As (5800) > N (14) > P (1). The aforementioned thermodynamic D(E-H) or $\Delta H_f°$ (EH_3) correlations predict a standard periodic trend; As should be faster than P, followed by N. Given the relative paucity of information on the actual thermodynamics of such events, high level quantum calculations were conducted.

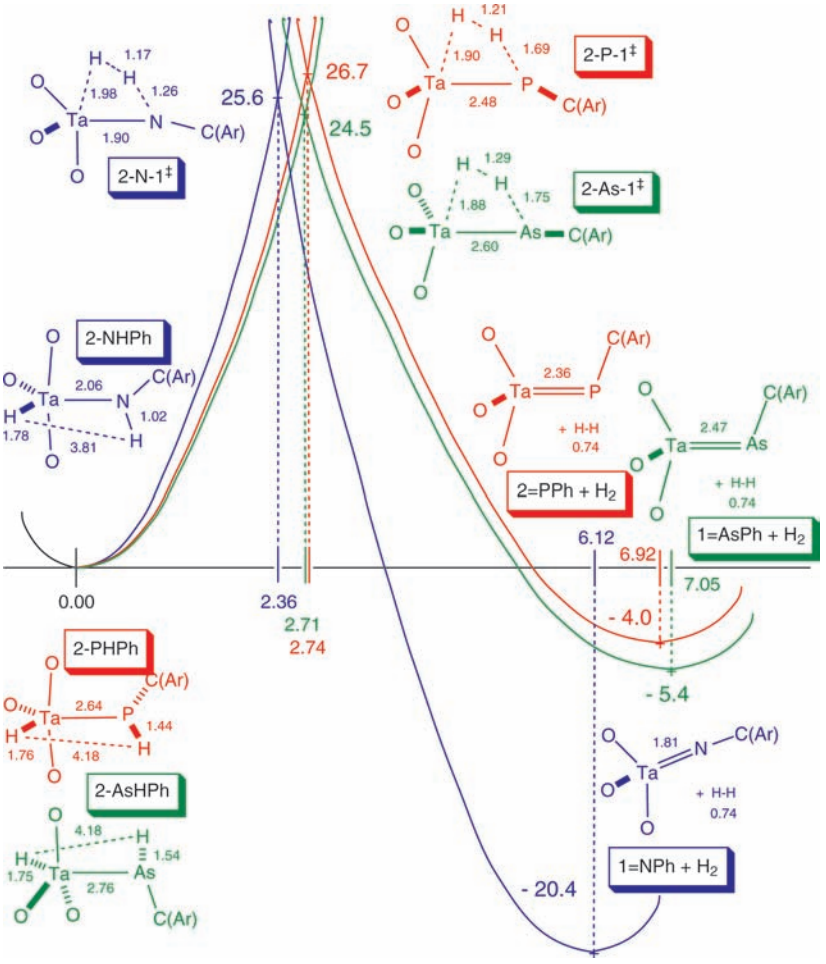

Figure 7. Calculated energies (y-axis, kcal/mol) of 1,2-H_2-elimination from (silox)$_3$HTaEHPh (**2**-EHPh; E = N, P, As) to give (silox)$_3$Ta=EPh (**1**=EPh, E = N, P, As) + H_2 via transition states [**2**-E-**1**]‡ (E = N, P, As). The reaction coordinate (x-axis) is described in Table 5 (RC(x)).

4. Calculations on 1,2-H_2-Elimination from (silox)$_3$-HTaEHR. Figure 7 reveals the geometries and relative energies of (silox)$_3$HTaEHPh (**2**-EHPh; E = N, P, As), the products (silox)$_3$Ta=EPh (**1**=EPh, E = N, P, As) + H_2, and intervening transition states [**2**-E-**1**]‡ (E = N, P, As). Remarkably, the calculations (24.8 °C: $\Delta G^‡$(P)$_{cald}$ = 26.7 kcal/mol, $\Delta G^‡$(N)$_{cald}$ = 25.6 kcal/mol, $\Delta G^‡$(As)$_{cald}$ = 24.5 kcal/mol) parallel the general experimental trend although the activation free energies are somewhat different (24.8 °C: $\Delta G^‡$(P) = 25.0 kcal/mol, $\Delta G^‡$(N) = 23.5 kcal/mol, $\Delta G^‡$(As) = 19.9 kcal/mol). One straightforward explanation for the lack of a periodic trend concerns the thermodynamics for 1,2-H_2-elimination, which is calculated to be 20.4 kcal/mol exoergic for N, but only 4.0 and 5.4 kcal/mol favorable for P and As, respectively. The greater favorable free energy for elimination of H_2 from the amide-hydride suggests a lower transition state than the P and As cases that have only a modest driving force.

The argument that the more favorable free energy change for N renders a lower transition state also suggests that [**2**-N-**1**]‡ should occur *earlier* in the reaction coordinate. Table 5 provides a view of the reaction coordinate parametrized solely via bond distance changes: (1) as a change in total bond lengths starting from (silox)$_3$HTaEHPh (**2**-EHPh; E = N, P, As; x = 0), given as RC(x); (2) as a fractional change in a reaction coordinate in bond length normalized to 1.00 with the pnictide-hydrides **2**-EHPh at 0.00. Somewhat surprisingly, the RC for all of the pnictogens is similar, where the TS is about 40% of the way to the product pnictidene (N, 0.39; P, 0.40; As, 0.38), despite a significant disparity in the sum of bond distance changes: N, 6.12 Å; P, 6.92 Å; As, 7.05 Å. One way to rationalize these features is to accept the premise that the Ta=N bond is likely to have a substantially greater force constant than the remaining Ta=P and Ta=As bonds, thus affording a "steeper sided" free energy surface (Figure 7) for the product **1**=NPh relative to **1**=PPh and **1**=AsPh (likely to be also true for **2**-EHPh). A steeper free energy surface would counteract the expectation of an earlier transition state for N because of the more favorable $\Delta G°$, while allowing the overall reaction coordinate to be more compressed. This can be observed in the changes in the pnictide and pnictidene distances. From **2**-EHPh to [**2**-E-**1**]‡, the Ta−E distances all change by −0.16 Å, but this is a far greater percentage change for the amide (7.8% relative to ~6% for P and As), while the percent change in d(TaE) from [**2**-E-**1**]‡ to **1**=EPh are all roughly 5% for all three cases. There is a corresponding greater percent change in the d(EH) for N > P > As that complements the d(TaE) explanation. Essentially, the greater bond strengths in the N species, especially that of the imido product, render the transition state later than it would be based solely on the standard free energy change for

Table 5. Calculated Reaction Coordinate[a] Changes from **2**-EHPh to [**2**-E-**1**]‡ to **1**=EPh

	d(TaH)	*d*(TaE)	*d*(EH)	*d*(HH)	∑d	RC(*x*)[b]	RC[c]
2-NHPh	1.78	2.06	1.02	3.81	8.67	0.00	0.00
Δ	0.20	−0.16	0.24	−2.47	−2.36		
[**2**-N-**1**]‡	1.98	1.90	1.26	1.17	6.31	2.36	0.39
Δ		−0.09		−0.43	−3.76		
1=NPh		1.81		0.74	2.55	6.12	1.00
2-PHPh	1.76	2.64	1.44	4.18	10.02	0.00	0.00
Δ	0.14	−0.16	0.25	−2.97	−2.74		
[**2**-P-**1**]‡	1.90	2.48	1.69	1.21	7.28	2.74	0.40
Δ		−0.12		−0.47	−4.18		
1=PPh		2.36		0.74	3.10	6.92	1.00
2-AsHPh	1.75	2.76	1.54	4.18	10.23	0.00	0.00
Δ	0.13	−0.16	0.21	−2.89	−2.71		
[**2**-As-**1**]‡	1.88	2.60	1.75	1.29	7.52	2.71	0.38
Δ		−0.13		−0.55	−4.34		
1=AsPh		2.47		0.74	3.18	7.05	1.00

[a] The reaction coordinate (RC) is roughly considered as the sum of the interatomic distances involved in the elimination; the product RC is simply defined as *d*(TaE) + *d*(HH). [b] The positional coordinate *x* indicates the total distance changes along the reaction coordinate. [c] The RC refers to the fraction of reaction progress relative to the pnictide-hydrides at 0.00.

1,2-H_2-elimination. Since the torsional motions of the atoms in the 1,2-H_2-elimination events are likely to parallel the bond strengths from the standpoint of energies (i.e., easier to bend X−E−H bonds as As(easier) < P < N), this parametrization of the RC is reasonable.

Dinitrogen Binding. 1. Collateral Discoveries. While the indirect synthesis of the hypothetical dinitrogen complex, [(silox)$_3$Ta]$_2$(μ-N_2) (**1$_2$**-N_2), which is likely to be a diimide,[7−9] has not been realized, several discoveries during the course of these investigations are noteworthy. The synthesis of (silox)$_3$Ta=C=PPh$_3$ (**1**=CPPh$_3$), for example, may permit examination of the reactivity of an incipient "(silox)$_3$TaC" (**1**-C) via phosphine dissociation. Preliminary indications are that carbonylation yields the known ketenylidene (silox)$_3$Ta=C=C=O (**1**=CCO), suggesting that loss of PPh$_3$ can occur under the right circumstances. The possibility of Wittig-like reactivity of the phosphaalkylidyne fragment is another plausible path of discovery; studies are ongoing.

In the history of silox-based chemistry from these laboratories, the loss of silanol, other than from degradative hydrolysis, had not been cleanly observed until the thermolysis of (silox)$_3$MeTaNHNH2 (**4**-NHNH$_2$) led to [(silox)$_2$TaMe](μ-$N_\alpha HN_\beta$)(μ-$N_\gamma HN_\delta$H)[Ta(silox)$_2$] (**5**). Unfortunately, the association of (silox)H with this complex, presumably via hydrogen bonding as solutions were concentrated, hampered purification of the unusual cyclic ditantalum species. Nonetheless, the loss of (silox)H via amination will be kept in mind as a future synthetic tool.

2. Compromise Diimide, [(silox)$_2$ClTa]$_2$(μ-N_2). The structure and stability of [(silox)$_2$ClTa]$_2$(μ-N_2) (**8**-Cl) leave little question that the hypothetical [(silox)$_3$Ta]$_2$(μ-N_2) (**1$_2$**-N_2) complex should be stable. Even though the crystallographic model precluded a true determination of *d*(TaN) and *d*(NN), the ditantalum interatomic distance of 4.874 Å is more consistent with two tantalum-imido interactions and an elongated dinitrogen distance than a bridging dinitrogen complex. Again, its stability with regard to dinitrogen loss supports the notion of the title quest.

3. Calculations on Dinitrogen Binding and Activation by (silox)$_3$Ta. Although [(silox)$_2$ClTa]$_2$(μ-N_2) (**8**-Cl) provides a potent example of the entitled dinitrogen activation, the forward reaction of N_2 + "(silox)$_2$ClTa" cannot be examined because the *bis*-siloxchloride tantalum monomer is not a stable entity; only (silox)$_3$Ta (**1**) has been shown to possess the necessary sterics coupled to a unique electronic, 3-coordinate environment to exist in monomer form.[4] As a consequence, high level quantum calculations were performed on the hypothetical dinitrogen activation illustrated in Scheme 1.

Figure 8 illustrates some of the complexity pertaining to dinitrogen activation by (silox)$_3$Ta (**1**, ^{n}Ta), first in binding N_2 to form (silox)$_3$TaN$_2$ (**1**-N_2, ^{n}Ta−N_2), and second to form the diimide (silox)$_3$Ta=N−N=Ta(silox)$_3$ (**1$_2$**-N_2, ^{n}Ta-NN-^{n}Ta) within the constraints of a *linear* reaction coordinate. 3-Coordinate **1** is a singlet (^{1}Ta, $(d_{z2})^2$) with *d*(TaO) of 1.89 Å and O−Ta−O angles of 120(1)° that is ∼19 kcal/mol below the triplet of nearest energy, ^{3}Ta, whose electronic configuration is $(d_{z2})^1(d_{xz}$ or $d_{yz})^1$, that is, ^{3}E″ in D_{3h}. Borrowing from previous calculations,[84] the barrier to convert from ^{1}Ta to ^{3}Ta is a few kcal/mol higher. Binding N_2 requires intersystem crossing to a triplet surface, as **1**-N_2 exists as a triplet that is 7.2 kcal/mol above the separated reagents, and ∼5.5 kcal/mol below its respective singlet. Triplet ^{3}Ta−N_2 possesses a *d*(TaN) of 1.96 Å, an elongated *d*(NN) of 1.18 Å (relative to the calculated 1.108 Å for free N_2), and a slightly pyramidalized core suggesting only modest reorganization energy. The electronic configuration of $d_{xz}{}^1d_{yz}{}^1$ for ^{3}Ta−N_2 ($^3A_2$ in C_{3v}) correlates with neither the ground state (GS) nor the first excited state (ES) of **1**, and suggests that a higher lying triplet ($^3A_2$″, red dashed line) must somehow be accessed for binding. In summary, *all transition states for* ^{n}Ta + N_2 → ^{n}Ta−N_2 *require intersystem crossing events that are forbidden by orbital symmetry*. Some also require spin crossovers, but previous calculations suggest that these are inconsequential, especially within second and third row transition metal systems.[83−88]

The second step, binding of (silox)$_3$TaN$_2$ (**1**-N_2, ^{3}Ta−N_2) to another (silox)$_3$Ta (**1**, ^{n}Ta) can be estimated to be roughly the same energy as the initial binding event, but the surface is now a quintet, since both tantalum centers are triplets. One possible way for (silox)$_3$Ta (**1**) to bind **1**-N_2 is to intersystem cross to the same triplet that may be necessary to bind N_2 in the first step (i.e., the dashed blue surface), incurring a large barrier in the process. Once the binding has occurred to give (silox)$_3$Ta−N_2-Ta(silox)$_3$ (**1$_2$**-N_2, ^{n}Ta-NN-^{n}Ta), electronic reorganization must occur to reach the singlet surface of the GS product. Since the diimide product (*d*(TaN) = 1.84 Å; *d*(NN) = 1.29 Å; ∠O−Ta−O = 109(1)°) is ∼55 kcal/mol lower than 2 **1** + N_2, orbital symmetry constraints may be more readily

(83) Veige, A. S.; Slaughter, L. M.; Lobkovsky, E. B.; Wolczanski, P. T.; Matsunaga, N.; Decker, S. A.; Cundari, T. R. *Inorg. Chem.* **2003**, *42*, 6204–6224.
(84) Carreon-Macedo, J. L.; Harvey, J. N. *J. Am. Chem. Soc.* **2004**, *126*, 5789–5797.
(85) (a) Poli, R. *J. Organomet. Chem.* **2004**, *689*, 4291–4304. (b) Poli, R. *Acc. Chem. Res.* **1997**, *30*, 1861–1866.
(86) (a) Harvey, J. N.; Poli, R.; Smith, K. M. *Coord. Chem. Rev.* **2003**, *238*, 347–361. (b) Poli, R.; Harvey, J. N. *Chem. Soc. Rev.* **2003**, *32*, 1–8.
(87) Harvey, J. N. *Struct. Bonding* **2004**, *112*, 151–183.
(88) Matsunaga, N.; Koseki, S. *Rev. Comput. Chem.* **2004**, *20*, 101–152.

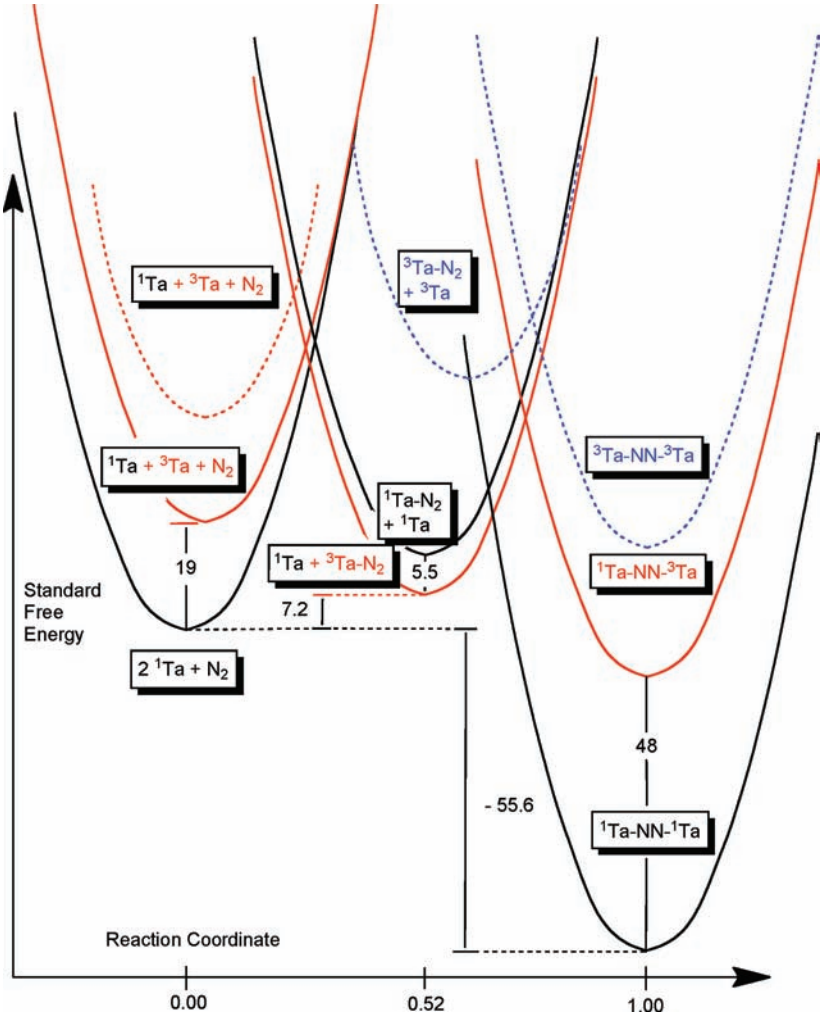

Figure 8. Plausible *linear* reaction coordinate (RC) versus standard free energy diagram for 2 $(silox)_3Ta$ (**1**) + N_2 ($(silox)_3Ta$ = ^{n}Ta) to hypothetical $(silox)_3TaN_2Ta(silox)_3$ (**1$_2$**-N_2, ^{n}Ta-NN-^{n}Ta) via $(silox)_3TaN_2$ (**1**-N_2, ^{n}Ta−N_2). Calculated standard free energies are in kcal/mol and the RC is based on the calculated *d*(TaN) and *d*(NN) changes, with all surface representations parabolically equivalent. The energies of species pertaining to dashed surfaces have been estimated.

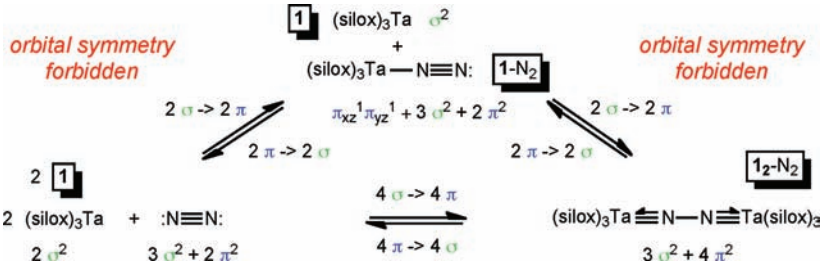

Figure 9. Simple illustration of orbital symmetry constraints in the conversion of 2 $(silox)_3Ta$ (**1**) + N_2 ($(silox)_3Ta$ = ^{n}Ta) to hypothetical $(silox)_3TaN_2Ta(silox)_3$ (**1$_2$**-N_2, ^{n}Ta-NN-^{n}Ta) via $(silox)_3TaN_2$ (**1**-N_2, ^{n}Ta−N_2).

overcome, *but the reduction of dinitrogen to diimide is also orbital symmetry forbidden from* ***1***-N_2.

It is clear from Figure 8 that the constraints of orbital symmetry must be overcome in both the initial and the second binding events of N_2. One way to overcome the electronic constraints depicted, that is, lower the intersystem crossing barriers, is to consider non-linear paths that effectively "mix" electron configurations that are intrinsically disparate, namely, those of σ-character with those of π-character. These paths are too varied to individually address without extensive calculations or additional evidence, but one reaction coordinate pertinent to the reorganization of $(silox)_3TaN_2Ta(silox)_3$ (**1$_2$**-N_2, ^{n}Ta-NN-^{n}Ta) has already been vetted.

The cleavage of N_2 by $(ArRN)_3Mo$ to GS singlet nitride products, 2 $(ArRN)_3MoN$, is orbital symmetry forbidden.[19−23] In this case, the binding of N_2 to form $[(ArRN)_3Mo]_2(\mu$-$N_2)$ is aided by the $S = 3/2$ states of the Mo(III) precursor, which require little promotional energy (to Mo(III) $S = 1/2$ states) to achieve the $S = 1$ state of the dinitrogen intermediate. Compared to the tantalum case, binding is readily accomplished, and it is

the *cleavage* of N_2 that is orbital symmetry forbidden. Scission eventually occurs because the parentage of only one orbital pair needs to be converted from π- to σ-character, and there is a considerably favorable free energy to aid in the process. In the tantalum case, each step (Figure 9) carries a significant energy penalty to overcome orbital symmetry constraints, either in changing electronic surfaces or in the significant reorganization energy required in lowering the symmetry to mix σ- and π-character.

Experimental Section

General Considerations. All manipulations were performed using either glovebox or high vacuum line techniques. All glassware was oven-dried. THF and ether were distilled under nitrogen from purple sodium benzophenone ketyl and vacuum transferred from the same prior to use. Hydrocarbon solvents were treated in the same manner with the addition of 1−2 mL/L tetraglyme. Benzene-d_6 and toluene-d_8 were dried over sodium, activated 4 Å molecular sieves, vacuum transferred, and stored under nitrogen. THF-d_8 was dried over sodium and vacuum transferred from sodium benzophenone ketyl prior to use. H_2 and D_2 were passed over a column containing activated 4 Å sieves and copper oxide. Primary amines, TMSCl, 1,4-cyclohexadiene, and phenylarsine oxide were purchased from Aldrich and dried over activated 4 Å sieves. NH_3 (Matheson) was dried over sodium and degassed prior to use. PH_3 (Matheson) was used as received. AsH_3 (***Caution! Danger, very toxic!***) was generated in small quantities from dilute mineral acid digestion of Zn_3As_2 (Cerac). Phenyl phosphine was purchased from Aldrich and used without further purification. (^{t}Bu$_3$SiO)$_3$Ta (**1**),[2] (^{t}Bu$_3$SiO)$_3$TaH$_2$ (**2**-H),[33] and phenyl arsine[89] were prepared following published procedures.

^{1}H, ^{13}C{^{1}H}, and ^{31}P NMR spectra were obtained on Varian XL-200 and XL-400, and Inova 400, 500 and 600 MHz spectrometers and chemical shifts are reported relative to benzene-d_6 (^{1}H, δ 7.15; ^{13}C{^{1}H}, δ 128.00) or external H_3PO_4 (^{31}P, δ 0.00). UV-vis spectra were acquired on a Hitachi U-2000 spectrometer, and IR spectra were recorded on a Mattson FT-IR, Perkin-Elmer 299B grating IR, or PE 377 grating IR. Combustion analyses were performed by Oneida Research Services (Whitesboro, NY), Robertson Microlit Laboratories (Madison, NJ), or Texas Analytical (Houston, TX). Molecular weight determinations via cryoscopy in benzene or vapor phase osmometry were performed on home-built instruments.

Procedures. 1. (^{t}Bu$_3$SiO)$_3$HTaNH$_2$ (2-NH$_2$). To a 10 mL flask containing 360 mg (silox)$_3$Ta (**1**, 0.435 mmol) was distilled 8 mL of hexanes at −78 °C. The flask was opened to a calibrated gas bulb containing NH_3 (0.456 mmol, 1.05 equiv) and allowed to warm to 23 °C with stirring. The initial blue color discharged completely after 30 min. Reduction of the volume to 3 mL, cooling to −78 °C, and filtration led to the isolation of 217 mg of white crystals (59%). Anal. Calcd. for $C_{36}H_{84}O_3NSi_3Ta$: C, 51.22; H, 10.03; N, 1.66. Found: C, 51.31; H, 10.04; N, 1.41.

2. (^{t}Bu$_3$SiO)$_3$HTaPH$_2$ (2-PH$_2$). To a 100 mL flask containing (silox)$_3$Ta (**1**, 0.341 g, 0.412 mmol) was distilled 50 mL of hexane at 77 K. PH_3 was condensed into the flask from a calibrated bulb (415 Torr in 91 mL, 2.06 mmol, 5 equiv), and the solution was allowed to warm slowly to 23 °C. The initial blue color faded to green, then yellow over a period of 30 min, and a red solid formed. After another 30 min, the excess PH_3 was removed, and the volume of the solution reduced to 10 mL. The solution was filtered, concentrated, and cooled to −78 °C, to yield pale yellow crystals (0.192 g, 54%). IR (nujol, cm^{-1}) 2285 (m), 2275 (m), 1775 (br, s), 1450 (m), 1375 (m), 1065 (w), 1010 (w), 1000 (w), 970 (w), 930 (w), 880 (br, s), 800 (br, s), 625 (s). M_r found: 858(68); calcd: 861. Combustion analysis was precluded by thermal instability.

3. (^{t}Bu$_3$SiO)$_3$HTaPHPh (2-PHPh). A 25 mL flask was charged with (silox)$_3$Ta (**1**, 0.682 g, 0.824 mmol), and 10 mL of pentane was added at −78 °C. Phenyl phosphine (90.7 μL, 0.825 mmol) was transferred into a separate flask, and 10 mL pentane was added at −78 °C. The solutions were warmed and stirred to ensure homogeneity. The solution of **1** was cooled to −78 °C, and the $PhPH_2$ solution was added via syringe in two portions. This mixture was stirred for 5 min and then warmed to 23 °C as a color change from blue to yellow-orange was observed (∼10 min); stirring was continued for another 10 min. The volatiles were removed, and pentane (10 mL) was added. The solution was filtered, concentrated to 5 mL, and cooled to −78 °C to afford bright yellow crystals (0.298 g, 39%). IR (nujol, cm^{-1}) 2320 (m), 1790 (br, s), 1580 (m), 1470 (s), 1375 (m), 1005 (w), 960−800 (br, s), 725 (m), 690 (m), 620 (s). Combustion analysis was precluded because of thermal instability.

4. (^{t}Bu$_3$SiO)$_3$Ta=NH (2=NH). A 100 mL flask was charged with **1** (0.979 g, 1.18 mmol), attached to a frit assembly, and evacuated. Hexane (50 mL) was added via vacuum transfer. 2-Methylaziridine (360 Torr in 91 mL, 1.79 mmol, 1.5 equiv) was added to the stirred solution at −78 °C. As the solution was warmed to room temperature, the blue color of the solution quickly faded to pale yellow. After stirring for 30 min the volatiles were removed and fresh hexane was added. The solution was filtered and concentrated to 10 mL. White crystals formed upon cooling to −78 °C and were isolated by filtration (0.771 g). A second crop was obtained in a like manner (0.080 g, 85% total). IR (nujol, cm^{-1}) 3470 (m), 1375 (m), 1010 (w), 935 (w), 880 (br, s), 820 (s), 630 (s). Anal. Calcd for $C_{36}H_{82}O_3NSi_3Ta$: C, 51.34; H, 9.81; N, 1.66. Found: C, 51.38; H, 10.09; N, 1.54.

5. (^{t}Bu$_3$SiO)$_3$Ta=NCH$_3$ (1=NCH$_3$). Into a glass bomb reactor was transferred a solution of (silox)$_3$Ta (**1**, 0.438 g, 0.529 mmol) in hexane (10 mL). The solution was freeze/pump/thaw degassed three times, and $MeNH_2$ was condensed in from a calibrated gas bulb (77 Torr in 125 mL, 0.53 mmol). As the bomb warmed to 23 °C, the blue color faded to pale yellow. After stirring for 12 h, the solution was frozen and a copious quantity of gas was evacuated from the bomb. The solution was again warmed and stirred. This cycle was repeated intermittently over a period of 3 d until no more gas was evolved. The resulting solution was concentrated to 4 mL, cooled to −78 °C, and filtered to yield a white powder (0.228 g, 50%). IR (nujol, cm^{-1}) 1475 (s), 1375 (m), 1320 (m), 1010 (w), 975 (m), 935 (w), 875 (br, s), 820 (s), 625 (s). Anal. Calcd for $C_{37}H_{84}O_3NSi_3Ta$: C, 51.90; H, 9.89; N, 1.64. Found: C, 51.79; H, 9.79; N, 1.45.

6. (^{t}Bu$_3$SiO)$_3$Ta=NPh (1=NPh). To a glass bomb reactor was added a solution of (silox)$_3$Ta (**1**, 0.486 g, 0.587 mmol) dissolved in 6 mL of benzene. Aniline (53.5 μL, 0.587 mmol) was dissolved in benzene (2 mL) and added to the bomb. This mixture was freeze/pump/thaw degassed three times and stirred at 23 °C for 6 h, during which time a generous quantity of gas evolved. The solution was degassed and warmed to 23 °C with continued stirring, and the process was repeated after an additional 12 h. The solution was then heated to 100 °C for 30 min and cooled to 23 °C. After the volatiles were removed, 15 mL of hexane was added, and the solution was degassed, filtered, and the volatiles removed. Ether (5 mL) was added, and the solution was cooled to −78 °C to afford white crystals (0.346 g, 64%). IR (nujol, cm^{-1}) 1590 (m), 1475 (s), 1385 (m), 1360 (s), 1010 (w), 985 (w), 950 (s), 875 (br, s), 820 (s), 750 (s), 685 (m), 620 (s). Anal. Calcd for $C_{42}H_{86}O_3NSi_3Ta$: C, 54.93; H, 9.44; N, 1.53. Found: C, 54.92; H, 9.45; N, 1.48.

7. (^{t}Bu$_3$SiO)$_3$Ta=N(C$_6$H$_4$-*p*-CF$_3$) (1=NC$_6$H$_4$-*p*-CF$_3$). A sample of (silox)$_3$Ta (**1**, 0.208 g, 0.251 mmol) was dissolved in 5 mL

(89) (a) Doak, G. O.; Freedman, L. D. *Organometallic Compounds of Arsenic, Antimony, and Bismuth*; Wiley-Interscience: New York, 1970. (b) Wiberg, K. B. *Z. Naturforsch.* **1957**, *12B*, 127–128.

of hexane and placed in a glass bomb reactor. Dihydrogen (~600 Torr at 77 K) was admitted to the reactor, and the solution was stirred at 23 °C for 20 h to ensure formation of $(silox)_3TaH_2$ (**2**-H), and degassed. In a glovebox, 4-aminobenzotrifluoride (31.6 μL, 0.252 mmol) was syringed into the hexane solution, which was degassed. After thermolysis in a wax bath at 90 °C for 10 h, the contents were transferred and the volatiles removed. Ether was added, and the solution was filtered. Concentration to 2 mL and cooling to −78 °C afforded white crystals (0.097 g, 39%). IR (Nujol, cm^{-1}) 1605 (m), 1510 (m), 1475 (s), 1375 (s), 1320 (s), 1200 (w), 1170 (m), 1160 (s), 1120 (s), 1110 (m), 1075 (m), 1010 (w), 960 (s), 880 (s, br), 840 (m), 820 (s), 645 (w), 635 (s). Anal. Calcd for $C_{43}H_{85}O_3F_3NSi_3Ta$: C, 51.14; H, 8.69; N, 1.42. Found: C, 52.62; H, 8.86; N, 1.31.

8. (^{t}Bu$_3$SiO)$_3$Ta=NLi (1=NLi). Glassware for this reaction was silylated in the following manner. After drying in an oven and cooling under vacuum, hexamethyldisilazane was introduced into a frit assembly against N_2 counterflow. The liquid was freeze/pump/thaw degassed three times and then warmed to reflux with a heat gun until it completely covered the inner surface of the glassware. The liquid was cooled and removed in vacuo, and the glassware transferred into a glovebox. One flask was charged with $(silox)_3Ta{=}NH$ (**1**=NH, 0.473 g, 0.562 mmol) and neopentyllithium (0.066 g, 0.845 mmol, 1.5 equiv). THF (25 mL) was transferred via vacuum transfer at −78 °C. The resulting solution went from yellow to colorless as it warmed to 23 °C, and after stirring for 1.5 h, the solution was filtered, concentrated to 5 mL, and cooled to −78 °C to afford colorless crystals (0.371 g, 78%). IR (nujol, cm^{-1}) 1460 (s), 1375 (s), 1010 (w), 900 (br, s), 820 (m), 625 (m). Anal. Calcd for $C_{36}H_{81}O_3NLiSi_3Ta$: C, 50.98; H, 9.63; N, 1.65. Found: C, 50.92; H, 9.84; N, 1.41.

9. (^{t}Bu$_3$SiO)$_3$Ta=NSiMe$_3$ (1=NTMS). A flask attached to a calibrated gas bulb was silylated as described above. The flask was charged with $(silox)_3Ta{=}NLi$ (**1**=NLi, 0.129 g, 0.152 mmol). THF (20 mL) was added at −78 °C followed by TMSCl (30 Torr in 91 mL, 0.15 mmol). Upon warming to 23 °C while stirring for 3 h, the volatiles were removed, and the solid was extracted into hexane. The solution was filtered, concentrated to 3 mL, and cooled to −78 °C, yielding white crystals (0.070 g, 50%). IR (nujol, cm^{-1}) 1475 (s), 1375 (m), 1245 (m), 1165 (s), 1010 (w), 950 (s), 870 (br, s), 820 (s), 745 (m), 630 (w), 625 (s). Anal. Calcd for $C_{40}H_{90}O_3NSi_4Ta$: C, 51.23; H, 9.92; N, 1.53. Found: C, 51.56; H, 9.94; N, 1.56.

10. (^{t}Bu$_3$SiO)$_3$Ta=PH (1=PH). A solution of **1** (0.476 g, 0.0.575 mmol) in hexane (50 mL) was exposed to 5 equiv of PH_3, which was admitted via a calibrated gas bulb. After stirring for 1 h, the solution was filtered and transferred to a glass bomb reactor, where it was freeze/pump/thaw degassed three times, warmed, and placed in an oil bath at 70 °C. After 2 h the solution was again frozen at 77 K and evacuated. A large quantity of gas was observed. The process was repeated until no more gas was evolved (two more cycles). The volatiles were removed, and 10 mL of hexane added. The solution was filtered, concentrated to 5 mL, and cooled to −78 °C, affording pale orange microcrystals (0.301 g, 61%). IR (nujol, cm^{-1}) 2150 (w), 1450 (m), 1375 (m), 1000 (w), 960 (m), 930 (w), 865 (s), 815 (m), 625 (m). M_r found: 857(50); calcd: 859. Anal. Calcd for $C_{36}H_{82}O_3PSi_3Ta$: C, 50.32; H, 9.62. Found: C, 50.32; H, 10.05.

11. (^{t}Bu$_3$SiO)$_3$Ta=PPh (1=PPh). The residue from the preparation of **2**-HPPh was dissolved in hexane and transferred into a glass bomb reactor. The contents were freeze/pump/thaw degassed three times. The bomb was warmed to 23 °C, and the solution stirred for 18 h. The bomb was degassed and immersed in a 55 °C bath. It was stirred for 3 d with intermittent degassing until gas evolution ceased and the solution was deep red. The volatiles were removed and 10 mL of pentane was added. The solution was transferred, concentrated to 3 mL, and cooled to −78 °C, yielding red-violet crystals (0.293 g, 62% based on remaining Ta). IR (nujol, cm^{-1}) 1580 (w), 1475 (m), 1375 (m), 1010 (w), 950 (m), 850 (s), 820 (m), 730 (w), 695 (w), 625 (m). Anal. Calcd for $C_{42}H_{86}O_3PSi_3Ta$: C, 53.93; H, 9.27. Found: C, 53.50; H, 9.44.

12. (^{t}Bu$_3$SiO)$_3$Ta=AsPh (1=AsPh). To a flask charged with **1** (0.615 g, 0.743 mmol) was distilled 10 mL of toluene at −78 °C. A solution of phenyl arsine (84.5 μL, 0.744 mmol) in toluene (5 mL) was added via syringe. The blue color of the solution faded noticeably after 15 min and changed to yellow-orange after 1 h. Stirring was continued for an additional hour, and upon warming, the solution effervesced and turned red, then green. After the reaction subsided, the volatiles were removed, and the residue was triturated three times with 5 mL of hexane. Hexane (10 mL) was added, and the solution was filtered. The residual was washed, and the filtrate was concentrated to 6 mL, and cooled to afford green microcrystals (0.511 g). A second crop was also isolated (0.109 g, 85% total). IR (nujol, cm^{-1}) 1576 (w), 1470 (m), 1375 (m), 1010 (w), 945 (s), 850 (br, s), 820 (s), 725 (w), 690 (w), 620 (m). M_r found: 980(45); calcd: 979. Anal. Calcd for $C_{42}H_{86}O_3Si_3AsTa$: C, 51.51; H, 8.85. Found: C, 51.17; H, 8.56.

13. (^{t}Bu$_3$SiO)$_3$Ta=AsH (1=AsH). Conducted on a Schlenk Line in a Hood. In a separate 2-neck flask attached to a needle valve and fitted with a bent tube containing solid Zn_3As_2 (34.4 mg, 0.0968 mmol, 1.2 equiv As) was frozen dilute sulfuric acid which was carefully degassed. The Zn_3As_2 was tapped into the acid at 0 °C to generate small quantities of AsH_3 (***Caution! Danger, Toxic***). The needle valve was opened and the AsH_3 was allowed to expand through a cold trap containing KOH and admitted to another flask attached to a frit assembly containing $(silox)_3Ta$ (**1**, 0.200 g, 0.242 mmol) in hexane at −78 °C. The solution became orange immediately and the evolution of a gas, presumably H_2 was noted, along with the formation of a red precipitate. The red solid was removed by filtration and dark orange crystals were obtained from the solution. ^{1}H NMR analysis revealed the material to be composed of $(silox)_3Ta{=}AsH$ (**1**=AsH) and $(silox)_3Ta(AsH_2)_2$ (**3**-$(AsH_2)_2$) in a 9:1 ratio. Any remaining AsH_3 was exposed to a cold NaOCl solution to oxidize the gas, and the Schlenk line was thoroughly evacuated through an LN_2 trap prior to further use.

14. (^{t}Bu$_3$SiO)$_3$Ta=CH$_2$ (1=CH$_2$). To a small bomb reactor containing **1** (2.01 g, 2.40 mmol), 690 mg of PPh_3CH_2 was added 40 mL of THF (40 mL). The reaction mixture was stirred for 1 h at 23 °C, degassed, and transferred for workup. The solution was filtered, concentrated to 15 mL, and cooled to −78 °C to afford 1.43 g (~70%) of yellow crystals that contained ~6% PPh_3 by mass. This was often sufficient for further reactions. Recrystallization from THF, then Et_2O, yielded pure yellow crystals (29%) that were submitted for EA. Anal. Calcd for $H_{83}C_{37}O_3Si_3Ta$: C, 52.83; H, 9.94. Found: C, 52.91; H, 9.84.

15. (^{t}Bu$_3$SiO)$_3$Ta=CPPh$_3$ (1=CPPh$_3$). To a 50 mL flask charged with **1** (1.96 g, 2.40 mmol) and 687 mg of PPh_3CH_2 at −78 °C was added 40 mL of THF by vacuum transfer. The solution was allowed to slowly warm to 23 °C over 12 h. The solution was degassed, filtered, concentrated to 15 mL, cooled to −78 °C, and filtered to yield 1.15 g **1**=CH_2 (58%). The filtrate residue was dissolved in 5 mL of pentane and cooled to −78 °C to yield 371 mg of an off-white powder identified (NMR) as an equimolar mixture of PPh_3 and **1**=$CPPh_3$. This material was dissolved in 5 mL of benzene and CH_3I (2 equiv, relative to PPh_3) was added and stirred overnight. A white precipitate was separated by filtration, and the solvent was removed in vacuo to yield 256 mg (10%, based on **1**) of **1**=$CPPh_3$ as a white powder. X-ray quality crystals could be grown from cooling a saturated pentane solution to −40 °C.

16. (silox)$_3$MeTaNHNH2 (4-NHNH$_2$). To a 10 mL round-bottom flask charged with **1**=CH_2 (560 mg, 0.665 mmol) and 8 mL of benzene was added 100 μL of hydrazine (3.1 mmol, 4.7 equiv) via syringe. The solution was stirred for 45 min, and

the solvent was removed in vacuo. The resultant off-white solid was triturated twice with 5 mL of THF, and 5 mL of pentane was added via vacuum transfer. The suspension was cold-filtered (−78 °C), and the filter cake washed with 5 mL of pentane. Upon removal of the volatiles, the residual was dissolved in 20 mL of benzene and filtered twice through Celite, each time followed by a 20 mL benzene wash. The filtrates were combined, and the solvent was removed in vacuo to yield 360 mg of **4**-$NHNH_2$ (49%) as a white powder. Anal. Calcd for $C_{37}H_{87}N_2O_3Si_3Ta$: C, 50.89; H, 10.04; N, 3.21. Found C, 50.94; H, 10.28; N, 3.09.

17. (silox)$_3$MeTaNH(-^{c}NCHMeCH$_2$) (4-NH(azir)). A 10 mL round-bottom flask was charged with 200 mg of **1**=CH_2 (0.24 mmol) and attached to a 180° valve adapter. The assembly was evacuated, and 2 mL of diethyl ether was added via vacuum transfer. To this solution was added 250 μL of *N*-amino-2-methylaziridine (3 mmol) at room temperature under argon counter-flow. The solution discolored over a period of 5 minutes, and the solvent and excess aziridine removed in vacuo, and the resulting waxy solid was left under dynamic vacuum for 45 min. The solid was recrystallized from pentane (0.5 mL) at −40 °C allowing for slow evaporation and washed with 0.5 mL of cold (−40 °C) pentane to yield 70 mg (32%) of a thermally sensitive waxy solid.

18. [(silox)$_2$TaMe](μ-N$_\alpha$HN$_\beta$)(μ-N$_\gamma$HN$_\delta$H)[Ta(silox)$_2$] (5). A small bomb was charged with 95 mg of **4**-$NHNH_2$ (0.11 mmol), and 2 mL of benzene was added. The bomb was heated to 75 °C for 24 h and subsequently evacuated of all volatiles. The resulting oil was dissolved in pentane, removed from the bomb, and placed in a 4-dram vial where the solvent was removed in vacuo to yield a slightly yellow liquid (90 mg, 95%). ^{1}H NMR analysis indicated complete conversion. The complex could not be separated from 2 equiv of ^{t}Bu$_3$SiOH, and was characterized by multinuclear NMR spectroscopy.

19. [(silox)$_3$MeTa](μ-η^2-*N*,*N*:η^1-*C*-NHNHCH$_2$CH$_2$CH$_2$)-[Ta(κ-O,C-OSi^{t}Bu$_2$CMe$_2$CH$_2$)(silox)$_2$] (7). To a resealable NMR tube was added 61 mg of **4**-NH(azir) (0.67 mmol) and 0.7 mL of C_6D_6. The tube was heated for 4 h at 80 °C until the starting material had disappeared. The resulting solution was removed from the tube and placed in a 1-dram vial, and a solution of (silox)$_3$Ta (58 mg in 1 mL. 0.070 mmol) was added. From the resulting green solution, yellow needles precipitated which were isolated by decanting the mother-liquor. The needles were washed with pentane and dried in vacuo to yield 15 mg of effectively insoluble material that could be recrystallized from hot THF (80 °C).

20. [(^{t}Bu$_3$SiO)$_2$TaCl]$_2$(μ-N$_2$) (8-Cl). To a 50 mL round-bottom flask containing 1.000 g of $[TaCl_3(THF)_2]_2N_2$ (1.12 mmol) and 1.09 g of sodium silox (4.56 mmol, 4.06 equiv) at −78 °C was added 25 mL of THF via vacuum transfer. The flask was allowed to warm to 23 °C over 18 h during which time the color changed from red-orange to yellow. The solvent was removed in vacuo, and 10 mL of pentane was added. Filtering the suspension, concentrating the solution to 5 mL, and cooling to −78 °C afforded yellow microcrystals which were dried in vacuo. After collection of a second crop the total yield was 828 mg (56%).

21. [(^{t}Bu$_3$SiO)$_2$TaMe]$_2$(μ-N$_2$) (8-Me). To a 25 mL flask charged with 100 mg of (0.075 mmol) $[(silox)_2TaCl]_2N_2$ at −78 °C was added 10 mL of Et_2O via vacuum transfer. After the solid dissolved, 0.08 mL of CH_3MgBr (2.0 M in Et_2O, 2.1 equiv) was added via syringe. The solution was allowed to warm to 23 °C over an 8 h period. After 30 min at 23 °C, a white precipitate formed, and the solution was filtered. The solution was filtered, concentrated to 2 mL, and cooled to −78 °C, affording a light-yellow powder that was collected by filtration and dried in vacuo (50 mg, 52%).

NMR Tube Reactions. General Procedures. Solid (^{t}Bu$_3$SiO)$_3$-Ta (**1**) or (^{t}Bu$_3$SiO)$_3$TaH$_2$ (**2**-H), typically 15−20 mg (0.017−0.025 mmol) was added to an NMR tube attached to a ground glass joint. Any solid reagents were also added along with deuterated solvent (∼0.6−0.8 mL). Liquid reagents were added via microliter syringe. The tube was attached to a needle valve, and the tube was degassed and sealed on a vacuum line. Any gaseous reagents were added via calibrated gas bulbs, and solvents were added to solid reagents via vacuum distillation prior to sealing.

22. (silox)$_3$HTaAsH$_2$ (2-AsH). Conducted on a Schlenk Line in a Hood. In a separate 2-neck flask attached to a needle valve and fitted with a bent tube containing solid Zn_3As_2 was frozen dilute sulfuric acid which was carefully degassed. The Zn_3As_2 was tapped into the acid at 0 °C to generate small quantities of AsH_3 (***Caution!*** *Danger, Toxic*). The needle valve was opened, and the AsH_3 was allowed to expand through a cold trap containing KOH and admitted to an NMR tube containing (silox)$_3$Ta (**1**), an equiv of 1,4-cyclohexadiene (added via vacuum transfer), and toluene-d_8. After the tube was sealed, any remaining AsH_3 was exposed to a cold NaOCl solution to oxidize the gas, and the Schlenk line was thoroughly evacuated through an LN_2 trap prior to further use. The NMR tube was kept at −78 °C for NMR monitoring.

General Kinetics. Solutions of (silox)$_3$HTaEHR (**2**-EHR) were generated in 2.0 mL volumetric flasks by one of three procedures: from isolated **2**-EHR and C_6D_6, dissolving (silox)$_3$-Ta (**1**) in C_6D_6 and adding REH_2 via syringe, or dissolving (silox)$_3$TaH$_2$ (**2**-H) in C_6D_6 and adding REH_2 via syringe. An exception was (silox)$_3$HTaNHMe (**2**-HNMe), which required addition of $MeNH_2$ from gas bulbs to individual tubes of **1** in C_6D_6. TMS_2O (∼0.5 μL) was added as an internal integration standard. The samples (∼0.6 mL) were transferred to NMR tubes sealed to 14/20 ground glass joints and attached to 180° needle valves. The tubes were freeze/pump/thaw degassed three times and sealed with a torch. Samples were kept in a constant temperature oven at 24.8(4)°C or were thermolyzed in a Tamson TX9 constant temperature bath (**2**-NH_2). The rate of disappearance of **2**-EHR was typically monitored via disappearance of the hydride ^{1}H NMR resonance (see Table 1 for exceptions) for 5−6 half-lives. Single-transient spectra were used for reproducibility of integration. In all cases where appearance of **1**=ER was monitored, the rate was found to be the same as disappearance of **2**-EHR. Rates and uncertainties were obtained from unweighted, non-linear, least-squares fitting of the exponential form of the rate expression (averaged where simultaneous runs were obtained).

Solutions of (silox)$_3$HTaAsPh (**2**-HAsPh) were generated in the following manner. $PhAsH_2$ was syringed into volumetric flasks which were then attached to needle valves. The flasks were cooled to 77 K, evacuated, and toluene-d_8 was added via vacuum transfer. The resulting solutions were added to NMR tubes containing **1** via vacuum transfer at 77 K, and 1,4-cyclohexadiene was added from gas bulbs. The tubes were sealed with a torch and maintained at 77 K until immediately prior to each run. The tubes were warmed to −78° in dry ice/acetone baths and agitated until the blue color of **1** had bleached. The samples were transferred to the NMR probe which had been previously cooled to −78 °C. Initial spectra were obtained to confirm the complete formation of **14**-AsHPh. The temperature of the probe was then raised to −9.5 °C and single-transient spectra were recorded at measured time intervals.

Single-Crystal X-ray Diffraction Studies. Upon isolation, the crystals were covered in polyisobutenes and placed under a 173 K N_2 stream on the goniometer head of a Siemens P4 SMART CCD area detector (graphite-monochromated Mo Kα radiation, λ = 0.71073 Å). The structures were solved by direct methods (SHELXS). All non-hydrogen atoms were refined anisotropically unless stated, and hydrogen atoms were treated as idealized contributions (Riding model).

23. (^{t}Bu$_3$SiO)$_3$Ta=NPh (1=NPh). A colorless block (0.3 × 0.3 × 0.4 mm) was obtained from a hot heptane solution, and was sealed in a 0.5 mm glass capillary. A total of 5077 reflections

were collected with 4665 being symmetry independent (R_{int} = 0.0254), and 3371 were greater than $2\sigma(I)$. A semiempirical absorption correction from equivalents was applied, and the refinement utilized $w^{-1} = \sigma^2(F_o^2) + (0.0549p)^2 + 7.4307p$, where $p = (F_o^2 + 2F_c^2)/3$. The ^{t}Bu groups of one silox group were disordered and modeled accordingly.

24. (^{t}Bu$_3$SiO)$_3$Ta=CPPh$_3$ (1=CPPh$_3$). A colorless block (0.15 × 0.20 × 0.25) was obtained from cooling a saturated pentane solution to −40 °C. A total of 73,173 reflections were collected with 17,745 being symmetry independent (R_{int} = 0.0766) and 12,757 were greater than $2\sigma(I)$. A semiempirical absorption correction from equivalents was applied, and the refinement utilized $w^{-1} = \sigma^2(F_o^2) + (0.0260p)^2 + 0.0173p$, where $p = (F_o^2 + 2F_c^2)/3$.

25. [(silox)$_3$MeTa](μ-η^2-*N*,*N*:η^1-CNHNHCH$_2$CH$_2$CH$_2$)[Ta(k-O,C-OSi^{t}Bu$_2$CMe$_2$CH$_2$)(silox)$_2$] (7). A colorless plate (0.03 × 0.10 × 0.20) was obtained from cooling a hot THF solution. A total of 57,689 reflections were collected with 17,150 being symmetry independent (R_{int} = 0.0762) and 11,852 were greater than $2\sigma(I)$. A semiempirical absorption correction from equivalents was applied, and the refinement utilized $w^{-1} = \sigma^2(F_o^2) + (0.0624p)^2 + 15.5864p$, where $p = (F_o^2 + 2F_c^2)/3$. Disordered solvent was SQEEZEd from the cell, and a disorder in the ^{t}Bu groups of one silox ligand was modeled appropriately.

26. [(^{t}Bu$_3$SiO)$_2$TaCl]$_2$(μ-N$_2$) (8-Cl). A colorless block (0.15 × 0.20 × 0.25) was obtained from slow evaporation of a 1:1 pentane/hexamethyldisiloxane solution at −78 °C over a period of 4 h. A total of 58,495 reflections were collected with 12,659 being symmetry independent (R_{int} = 0.0686), and 8,578 were greater than $2\sigma(I)$. A semiempirical absorption correction from equivalents was applied, and the refinement utilized $w^{-1} = \sigma^2(F_o^2) + (0.0605p)^2 + 73.4015p$, where $p = (F_o^2 + 2F_c^2)/3$. The disorder in the ^{t}Bu groups of one silox was modeled appropriately. The electron density in the region between the two tantalums did not refine well, and the nitrogen atoms were refined isotropically. The distances and angles between the two tantalums are inadequately determined (see text).

Calculations. To obtain minima for these complexes, full geometry optimizations, without any metric or symmetry restrictions, were performed using the Gaussian 03[90] package, and these employed density functional theory (DFT), specifically the BLYP functional.[91] Atoms were described with the Stevens effective core potentials (ECPs) and attendant valence basis sets (VBSs).[92] This scheme, dubbed CEP-31G(d), entails a valence triplet zeta description for the transition metals, a double-ζ-plus-polarization basis set for main group elements, and the −31G basis set for hydrogen. This level of theory was selected on the basis of previous work.[18,83]

Acknowledgment. P.T.W. thanks the NSF (CHE-0718030) and Cornell University, and TRC the DOE (DE-FG02-03ER15387) for financial support.

Supporting Information Available: CIF files for **1**=NPh, **1**=CPPh$_3$, **7**, and **8**-Cl. This material is available free of charge via the Internet at http://pubs.acs.org.

(90) Frisch, M. J. et al. *Gaussian 03*; Gaussian, Inc.: Pittsburgh PA, 1998.
(91) Parr, R. G.; Yang, W. *Density-functional Theory of Atoms and Molecules*; Oxford University Press: Oxford, 1989.
(92) Stevens, W. J.; Krauss, M.; Basch, H.; Jasien, P. G. *Can. J. Chem.* **1992**, *70*, 612–630.